Table II-2-2 Specifications of ground geophysical survey instruments

Name	Model	Manufacturer (Country)	Specifications
Magnetic Susceptibility Meter (Kappameter)	KT-5	Geofyzika Brno (Czechoslovakia)	Sensitivity; $1x10^{-5}$SI units, Range; $9.99x10^{-3}$, $99.9x10^{-3}$, $999x10^{-3}$SI units (automatically switched) Display; 4-digit LCD, Data memory; upto 12 measurements Dimensions; φ65x187mm
Scintillation Counter	GIS-5	Scintrex Limited (Canada)	Detector; NaI(Tl) crystal, Crystal volume; 5 $inch^3$ (82cc), Crystal dimensions; Near-cubic, 1.6"x1.6"x1.96", Energy thresholds; T.C.:>0.05 MeV, K+U+Th:>1.38 MeV, U+Th:>1.66 MeV, Th+Cal:>2.44 MeV, Counting periods; 1,3,10,30 or 100 seconds, Digital display; 19,999, Temperature; -20 ℃ to + 55℃, Dimensions; 250x190x95mm, Weight; 2.8 kg

Table II-2-3 Specifications of laboratorial measurement of geophysical property

Name	Model	Manufacturer (Country)	Specifications
Magnetic Susceptibility Meter	3101A	Bison (U.S.A.)	Sensitivity; $1x10^{-6}$SI units, Range; 10^{-6}～10^{-2} or 10^{-5}～10^{-1}SI units
Scintillation Counter	GIS-5	Scintrex Limited (Canada)	Detector; NaI(Tl) crystal, Crystal volume; 5 $inch^3$ (82cc), Crystal dimensions; Near-cubic, 1.6"x1.6"x1.96", Energy thresholds; T.C.:>0.05 MeV, K+U+Th:>1.38 MeV, U+Th:>1.66 MeV, Th+Cal:>2.44 MeV, Counting periods; 1,3,10,30 or 100 seconds, Digital display; 19,999, Temperature; -20 ℃ to + 55℃, Dimensions; 250x190x95mm, Weight; 2.8 kg

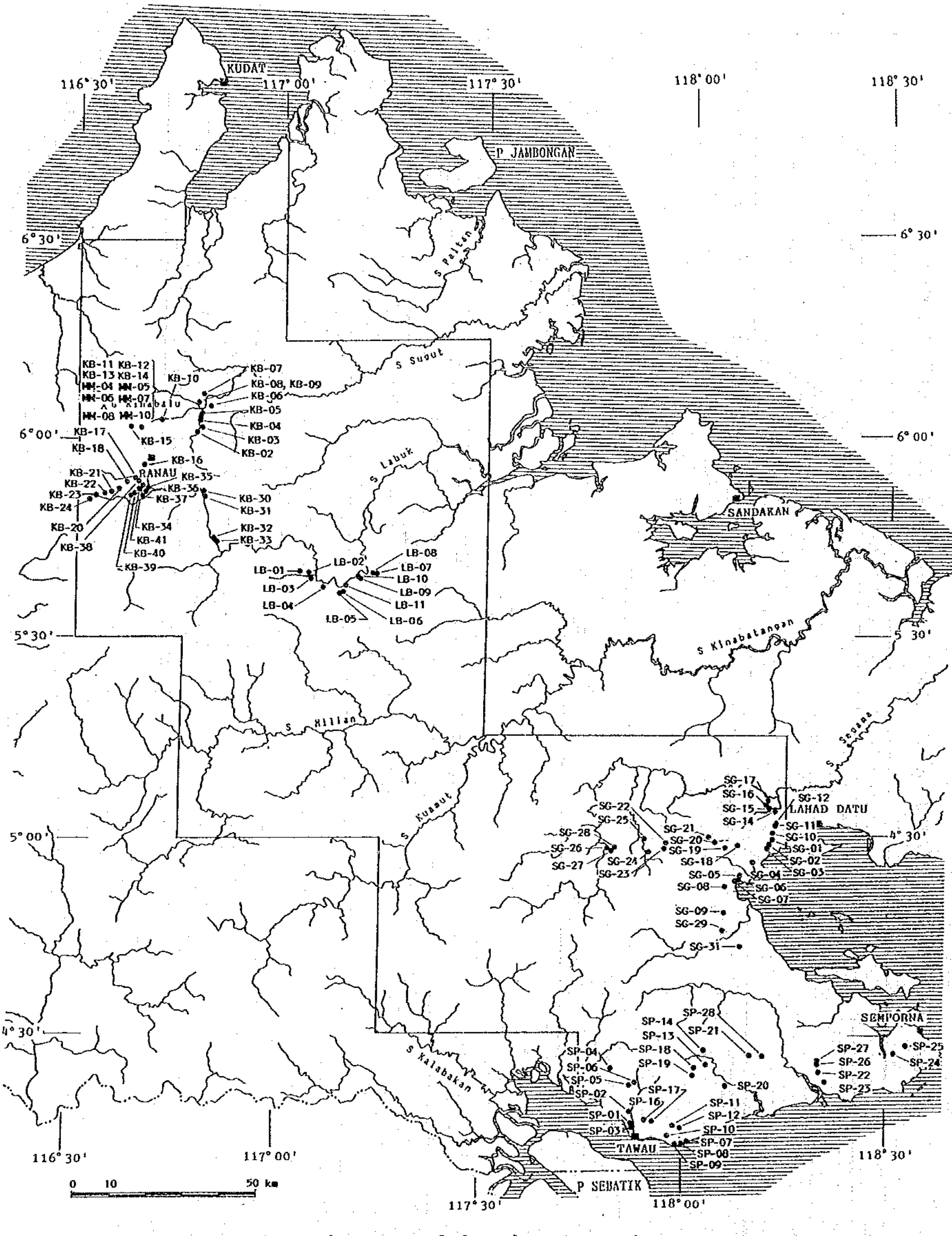

Fig. II-2-2 Location map of in-situ magnetic and radiometric measuring points

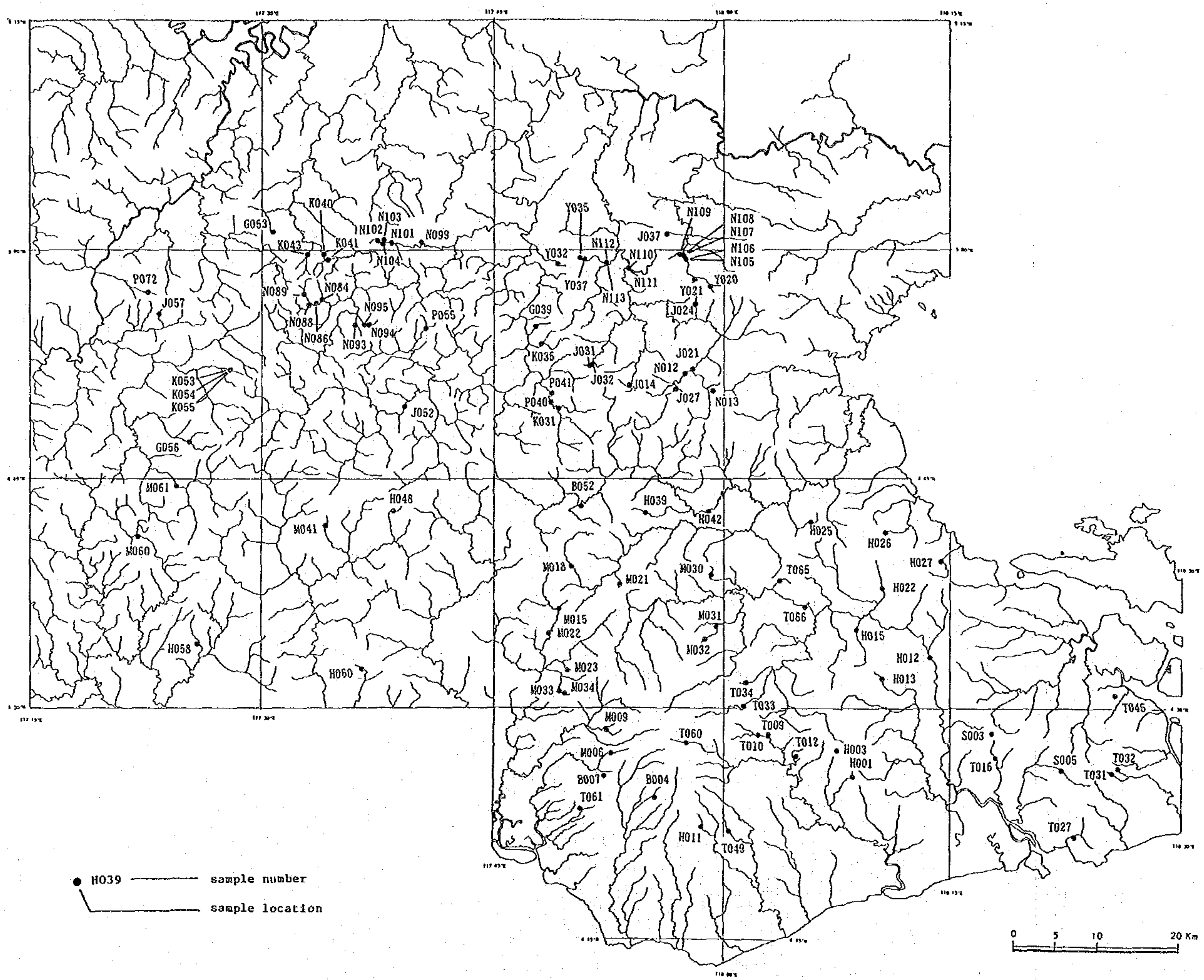

Fig. II-2-3 Location map of laboratorial magnetic and radiometric measurement samples in the Segama and Semporna area

2-4-2 Aeromagnetic and aero-radiometric data

(1) Total field magnetics

The aeromagnetic data were corrected for diurnal variations by adjustment with the recorded base station magnetic values. Where needed, the magnetic tie line results were used to further level the magnetic data. No corrections for regional variations were applied. The corrected profile data were interpolated on to a regular grid using an Akima spline technique. The grid provided the basis for threading the presented contours. A grid cell size of 100m was used.

"Total field magnetic" maps for five areas, Southern Kinabalu, Labuk, Segama, Northern Semporna and Southern Semporna, are shown in Figs.II-2-5, II-2-6, II-2-13, II-2-14 and II-2-15, respectively.

(2) Total Count of radiometric maps

Four channels of radiometric data(Total Count, K, U, and Th) are subject to a four stage data correction process. The stages are

① Low pass filter(seven point Hanning)

② Background removal

③ Terrain clearance correction

④ Compton stripping correction

Variations in radiometric backgrounds were removed by manual adjustments made after inspection of preliminary contour maps.

The Compton stripping factors used were

alpha	0.35(Th into U)	a	0.09(K into Th)
beta	0.30(Th into K)	b	0.00(K into Th)
gamma	0.73(U into K)	g	0.03(K into U)

where alpha, beta and gamma are the forward stripping coefficients and a, b and g are the backward stripping coefficients. these coefficients are taken in part from the sample checks done at the start of each flight.

The altitude attenuation coefficients used were 0.0072(TC), 0.0085 (K), 0.0082(U) and 0.0067(Th)/feet. These coefficients are taken from Geological Survey of Canada publications for similar radiometric systems.

Radiometric data were corrected to a mean sensor terrain clearance of about 145m. This has resulted in an amplification of the corrected count rates by factors 2.37(Total Count), 2.77(K), 2.67(U) and 2.23(Th) from those which would be seen at the nominal survey clearance of 180 m. Total count radiometric maps showing 2370 counts per second(pcs) for example would correspond to a raw count rate on the analog records of about 1000 cps.

The corrected data were interpolated on a square grid(grid cell size 100 m) using an Akima spline technique. The grids provides the basis for threading the presented contours.

"Radiometric Total Count" maps for five areas, Southern Kinabalu, Labuk, Segama, Northern Semporna and Southern Semporna, are shown in Figs.II-2-8, II-2-9, II-2-17, II-2-18 and II-2-19, respectively.

(3) Ternery map

The ternery maps are made from the gridded Pattasium, Uranium and Thorium data. Each data type is assigned a colour - red(Pottasium), yellow(Uranium) and blue(thorium). The intensity of colour assigned to each grid cell is varied according to relative amplitude. The highest Pottasium count rates are assigned the most intense red. The lowest Pottasium count rates are assigned the least intense red - almost white. The three colour maps are then over printed.

Variations in colour intensity on the ternery map should mimic the Total Count contour map. Variations in colour hue are variations in the relative surface radio-element geochemistry. A reddish area is relatively high in Pottasium. A yellowish area is relatively high in Uranium. A bluish area is relatively high in thorium. In theory, the neutral colour (equal relative amounts of K, U and Th) is grey to black - it is colourless.

Ternery maps for five areas, Southern Kinabalu, Labuk, Segama, Northern Semporna and Southern Semporna, are shown in Figs.II-2-10, II-2-11, II-2-20, II-2-21 and II-2-22, respectively.

2-5 Survey results

2-5-1 Ground survey and loboratorial measurement

(1) Ground Survey

Averages of magnetic susceptibilities and radioactivities, and the number of measuring points of 24 kinds of rocks are shown in Table II-2-4.

Rocks of high magnetic susceptibility of more than 10^{-3}CGSemu are gabbro, serpentinite, basalt, andesite, amphibolite, biotite hornfels, adamellite, granodiorite and tuff, which will induce magnetic anomalies of large amplitudes on Total Field Magnetics Maps.

High count radiometric rocks of more than 100 cps are sandstone, shale, biotite hornfels, adamellite and granodiorite, which will generate high-count radiometric anomalies on Total Count Radiometrics Maps.

High magnetic and high count rocks such as biotite hornfels, adamellite and granodiorite will cause large-amplitude magnetic anomalies and high-count radiometric anomalies at the same locations.

(2) Laboratorial measurement

Averages of magnetic susceptibilities and radioactivities, and the number of samples of 28 kinds of rocks are shown in Table II-2-5.

The magnetic susceptibilities show the similar results as those of the ground survey. Amphibolite, shale, gneiss, granodiorite, dolerite, andesite and basalt show high magnetic susceptibility of more than 10^{-3}CGSemu, which will induce magnetic anomalies of large amplitude on a Total Field Magnetics Maps.

While, the results of radioactivity measurements are not satisfied, because the volume of each rock sample seem not to be enough large to measure radioactivities.

2-5-2 Aeromagnetic and aero-radiometric data

As shown in Fig.II-2-4, a magnetic anomly due to highly magnetized prism model near the equator shows predominant nagative part above a prism and small positive parts at the south and north of a prism, and extends towards east and west. Quality analysis for magnetic anomalies should be made taking this characteristics of magnetic anomaly pattern into consideration.

Table II-2-4 Results of radiometric count and magnetic susceptibility in the field (κ)

Ser. No.	Geologic unit	Lithology	Average (No.) (Upper), Minimum - Maximum (Lower)				
			Total count (cps)	K+U+Th (cps)	U+Th (cps)	Th (cps)	κ ($\times10^{-3}$CGSemu)
1	Cb	Amphibolite	32.9 (2)	1.42 (2)	1.12 (2)	0.68 (2)	5.82 (2)
			17.8 - 48.0	1.09 - 1.75	0.89 - 1.35	0.63 - 0.73	0.64 - 11.0
2	Cb	Schist/	21.5 (5)	1.09 (5)	0.89 (5)	0.76 (5)	0.93 (5)
		Gneiss	11.2 - 45.0	1.00 - 1.33	0.75 - 1.06	0.61 - 0.82	0.34 - 2.28
3	KMb	Limestone	11.7 (1)	0.41 (1)	0.37 (1)	0.24 (1)	0.03 (1)
4	I_1	Gabbro	13.7 (4)	1.00 (4)	0.79 (4)	0.67 (4)	50.7 (4)
			5.00 - 36.5	0.79 - 1.35	0.69 - 0.91	0.63 - 0.71	0.60 - 163.
5	I_1	Serpentinite	15.4 (14)	1.03 (14)	0.76 (14)	0.67 (14)	23.2 (14)
			4.03 - 80.1	0.62 - 2.96	0.61 - 0.88	0.57 - 0.75	1.89 - 96.5
6	KpCs	Basalt	13.7 (6)	0.91 (6)	0.80 (6)	0.66 (6)	10.1 (6)
			9.03 - 21.8	0.75 - 1.23	0.70 - 0.88	0.53 - 0.77	0.51 - 21.1
7	KpCs	Chert	19.7 (3)	1.00 (3)	0.80 (3)	0.70 (3)	0.91 (3)
			14.6 - 23.7	0.94 - 1.03	0.70 - 0.98	0.64 - 0.75	0.08 - 2.48
8	KpCs	Sandstone	95.9 (3)	2.92 (3)	1.63 (3)	0.75 (3)	0.17 (3)
			92.2 - 100.	2.61 - 2.99	1.51 - 1.70	0.67 - 0.80	0.13 - 0.23
9	P_1Ts	Philite	186. (8)	5.20 (8)	2.59 (8)	1.03 (8)	0.19 (8)
			148. - 222.	4.48 - 5.99	2.13 - 3.01	0.81 - 1.13	0.10 - 0.33
10	P_1Ts	Shale	170. (3)	4.80 (3)	2.23 (3)	0.87 (3)	0.23 (3)
			159. - 184.	4.14 - 5.14	2.13 - 2.43	0.80 - 0.91	0.19 - 0.27
11	P_1Ts	Sandstone	139. (8)	4.10 (8)	2.14 (8)	0.88 (8)	0.14 (8)
			105. - 195.	3.15 - 5.11	1.81 - 2.45	0.77 - 1.10	0.08 - 0.22
12	P_4Gr	Sandstone	97.2 (6)	2.49 (6)	1.47 (6)	0.70 (6)	0.20 (6)
			73.2 - 115.	1.95 - 3.23	1.25 - 1.69	0.52 - 0.84	0.10 - 0.22
13	P_4Kg	Tuff	33.8 (2)	1.36 (2)	1.01 (2)	0.82 (2)	12.49 (2)
			33.8 - 33.8	1.36 - 1.36	1.01 - 1.01	0.82 - 0.82	7.87 - 17.1
14	P_4Kg	Limestone	17.7 (1)	0.90 (1)	0.70 (1)	0.60 (1)	0.04 (1)
15	P_4Km	Tuff	67.8 (1)	1.72 (1)	1.05 (1)	0.67 (1)	2.94 (1)
16	P_4Km	Basalt lava	32.6 (1)	0.96 (1)	0.82 (1)	0.62 (1)	28.4 (1)
17	P_4Km	Sandstone	73.3 (3)	1.92 (3)	1.24 (3)	0.58 (3)	0.18 (3)
			50.8 - 88.7	1.43 - 2.29	0.83 - 1.49	0.44 - 0.74	0.07 - 0.30
18	I_2	Biotite	200. (3)	5.62 (3)	2.07 (3)	0.97 (3)	18.8 (3)
		Hornfels*	191. - 216.	5.28 - 6.02	1.90 - 2.17	0.88 - 1.10	2.97 - 34.0
19	I_2	Adamellite	186. (7)	4.99 (7)	2.34 (7)	1.04 (7)	5.81 (7)
			132. - 283.	3.81 - 5.79	1.80 - 2.97	0.80 - 1.32	0.33 - 31.4
20	I_2	Granodiorite	175. (2)	4.40 (2)	2.13 (2)	0.82 (2)	1.59 (2)
			173. - 176.	4.38 - 4.42	1.97 - 2.28	0.80 - 0.83	1.51 - 1.67
21	I_3	Microdiorite	119. (3)	3.28 (3)	1.74 (3)	0.81 (3)	32.7 (3)
			95.5 - 149.	2.87 - 3.65	1.50 - 1.92	0.80 - 0.82	31.0 - 35.9
22	I_5	Andesite	82.4 (13)	2.35 (13)	1.37 (13)	0.73 (13)	14.3 (13)
			53.6 - 134.	1.75 - 3.95	1.06 - 2.17	0.61 - 0.99	0.10 - 27.4
23	I_6	Dacite	94.7 (3)	2.96 (3)	1.65 (3)	0.75 (3)	19.6 (3)
			74.7 - 115.	2.37 - 3.47	1.45 - 1.63	0.60 - 0.83	0.17 - 31.4
24	I_6	Basalt	73.7 (4)	2.41 (4)	1.34 (4)	0.71 (4)	5.72 (4)
			55.5 - 83.8	2.00 - 3.15	1.14 - 1.49	0.49 - 0.82	1.51 - 9.77

* Ore

Table II-2-5 Results of laboratorial radiometric count and magnetic susceptibility (κ)

Ser. No.	Geologic unit	Lithology	Average (No.) (Upper), Minimum - Maximum(Lower)				
			Total count (cps)	K+U+Th (cps)	U+Th (cps)	Th (cps)	κ ($\times 10^{-3}$CGSemu)
1	Cb	Amphibolite	3.0 (4) 1.17 - 4.78	0.73 (4) 0.10 - 1.53	0.40 (4) 0.40 - 0.44	0.33 (4) 0.12 - 0.44	0.98 (4) 0.110 - 2.391
2	Cb	Gneiss/ Schist	3.2 (5) 1.93 - 4.97	0.72 (5) 0.26 - 0.89	0.38 (5) 0.12 - 0.69	0.34 (5) 0.17 - 0.53	2.16 (5) 0.306 - 5.968
3	Cb	Granodiorite	5.0 (2) 3.97 - 5.95	0.80 (2) 0.54 - 1.06	0.20 (2) 0.17 - 0.23	0.44 (2) 0.35 - 0.52	1.99 (2) 0.084 - 3.897
4	Cb	Dolerite	1.7 (2) 1.42 - 2.50	0.91 (2) 0.89 - 0.93	0.22 (2) 0.17 - 0.26	0.30 (2) 0.20 - 0.39	1.19 (2) 0.786 - 1.593
5	Cb	Phyllite	2.91 (1)	0.84 (1)	0.52 (1)	0.06 (1)	0.098 (1)
6	Ub	Gabbro	3.5 (6) 1.75 - 2.50	0.47 (6) 0.13 - 0.94	0.40 (6) 0.10 - 0.59	0.32 (6) 0.08 - 0.55	1.69 (6) 0.349 - 4.935
7	Ub	Dolerite	3.9 (5) 1.65 - 5.26	0.71 (5) 0.32 - 1.58	0.71 (5) 0.49 -1.07	0.28 (5) 0.15 - 0.44	1.54 (6) 0.344 - 2.565
8	Ub	Peridotite	1.3 (4) 0.55 - 3.03	0.59 (4) 0.38 - 0.85	0.37 (4) 0.16 - 0.51	0.33 (4) 0.22 - 0.39	1.32 (4) 0.174 - 2.432
9	I_1	Andesite	4.9 (7) 3.00 - 7.94	0.74 (7) 0.60 - 1.21	0.50 (7) 0.15 - 0.89	0.40 (7) 0.13 - 0.84	3.01 (7) 0.722 - 4.503
10	I_1	Microdiorite	4.7 (3) 4.07 - 5.29	1.20 (3) 0.72 - 1.75	0.56 (3) 0.36 - 0.79	0.27 (3) 0.11 - 0.48	2.09 (3) 0.746 - 3.217
11	I_1	Coarse-Med. Tuff	5.4 (2) 3.30 - 7.40	0.66 (2) 0.36 - 0.96	0.64 (2) 0.56 - 0.71	0.22 (2) 0.18 - 0.25	1.31 (2) 0.986 - 1.632
12	I_1	Fine Tuff	9.83 (1)	0.66 (1)	0.26 (1)	0.63 (1)	0.069 (1)
13	I_1	Dacite	1.54 (1)	0.68 (1)	0.45 (1)	0.11 (1)	0.081 (1)
14	I_1	Altered Rock	5.8 (3) 3.35 - 7.21	0.71 (3) 0.56 - 0.80	0.45 (3) 0.11 - 0.96	0.24 (3) 0.14 - 0.42	0.16 (3) 0.043 - 0.378
15	KpCs	Basalt	2.8 (2) 2.35 - 3.28	0.85 (2) 0.84 - 0.85	0.56 (2) 0.54 - 0.57	0.29 (2) 0.24 - 0.33	2.85 (2) 1.096 - 4.603
16	KpCs	Shale	1.6 (2) 0.38 - 2.86	0.60 (2) 0.22 - 0.97	0.29 (2) 0.27 - 0.30	0.41 (2) 0.21 - 0.61	1.29 (2) 1.107 - 1.477
17	KpCs	Sandstone	2.6 (3) 2.29 - 3.13	0.51 (3) 0.24 - 0.67	0.70 (3) 0.63 - 0.84	0.15 (3) 0.00 - 0.41	0.22 (3) 0.066 - 0.272
18	KpCs	Chert	4.3 (3) 2.09 - 8.59	0.66 (3) 0.32 - 0.88	0.47 (3) 0.35 - 0.57	0.34 (3) 0.22 - 0.41	0.28 (3) 0.072 - 0.699
19	KpCs	Green Rock	2.34 (1)	0.62 (1)	1.03 (1)	0.40 (1)	3.107 (1)
20	P_4Kg	Tuff	3.9 (2) 3.77 - 4.05	0.64 (2) 0.41 - 0.86	0.26 (2) 0.09 - 0.43	0.39 (2) 0.30 - 0.47	1.85 (2) 1.601 - 2.095
21	P_4Kg	Sandstone	2.7 (3) 0.59 - 4.19	0.55 (3) 0.23 - 0.84	0.19 (3) 0.00 - 0.42	0.41 (3) 0.36 - 0.52	1.56 (3) 1.344 - 1.934
22	P_4Kg	Siltstone	1.9 (2) 0.47 - 3.37	0.59 (2) 0.59 - 0.59	0.20 (2) 0.00 - 0.39	0.35 (2) 0.25 - 0.44	0.074 (2) 0.062 - 0.086
23	P_4Kl	Shale/ Siltstone	5.0 (2) 2.80 - 7.10	1.02 (2) 0.94 - 1.09	0.51 (2) 0.46 - 0.55	0.42 (2) 0.26 - 0.57	0.066 (2) 0.031 - 0.070
24	P_4Km	Sandstone	4.2 (20) 1.16 - 7.24	0.60 (20) 0.00 - 1.18	0.44 (20) 0.11 - 0.86	0.33 (20) 0.02 - 0.69	0.109 (20) 0.051 - 0.856
25	P_4Km	Tuff.	5.91 (1)	0.89 (1)	0.22 (1)	0.51 (1)	3.341 (1)
26	P_4Km	Mudstone	3.9 (2) 1.83 - 5.91	0.77 (2) 0.50 - 1.04	0.32 (2) 0.27 - 0.37	0.39 (2) 0.27 - 0.50	0.587 (2) 0.402 - 0.772
27	I_2	Basalt	3.4 (5) 2.77 - 4.45	0.54 (5) 0.06 - 0.83	0.41 (5) 0.25 - 0.77	0.38 (5) 0.08 - 0.71	0.902 (5) 0.124 - 2.205
28	I_2	Andesite	5.4 (3) 4.73 - 5.80	0.87 (3) 0.55 - 1.37	0.26 (3) 0.00 - 0.69	0.30 (3) 0.17 - 0.38	2.54 (3) 2.167 - 3.275

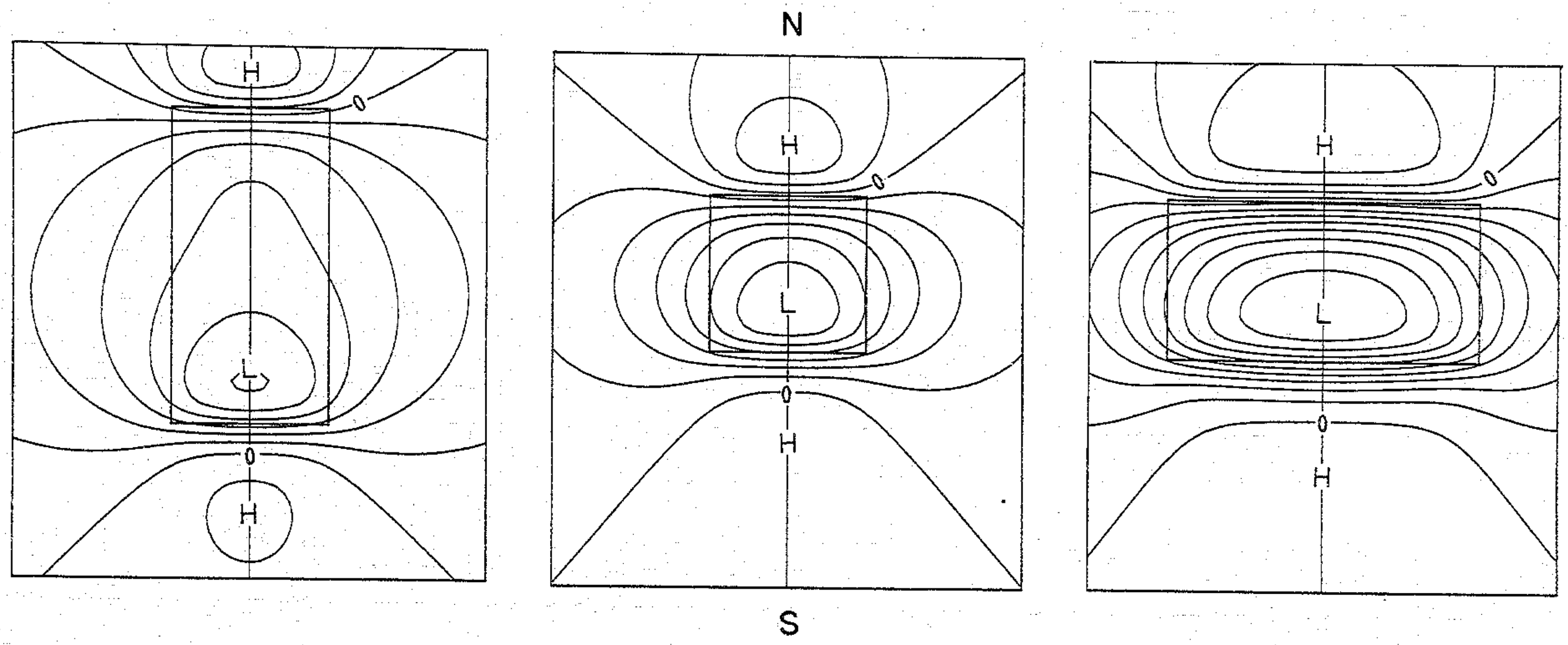

Fig. II-2-4 Theoretical magnetic anomaly due to prism model

As a quantative analysis, an automatic curve matching method by means of an electronic computer was applied to estimate quantatively the depth, size and magnetic susceptibility of anomalous body, comparing the observed with the calculated model curves.

In the following sections, the Southern Kinabalu and Labuk areas, and the Segama and Northern and Southern Semporna areas are called "Southern Kinabalu and Labuk area" and "Segama and Semporna area", respectively.

Magnetic anomaly maps of the Southern Kinabalu and Labuk area and the Segama and Semporna area are shown in Figs.II-2-7 and II-2-16, respectively, in which highly magnetized rocks and magnetic discontinuity lineaments are delineated qualitatively and quantitatively from "Total Field Magnetics" maps.

Radiometric anomaly maps of the Southern Kinabalu and Labuk area and the Segama and Semporna area are shown in Figs.II-2-12 and II-2-23, respectively, in which distribution area of high count anomalies of Total Count(T.C.), Pottasium(K), Uranium(U) and Thorium(Th) radiomerics are shown, and radiometric discontinuity lineaments are delineated qualitatively from "Total Count Radiometric Contours" and "Ternery Map".

(1) Southern Kinabalu and Labuk area

① Magnetic anomaly map

Total field magnetic maps of the Southern Kinabalu and Labuk areas are shown in Figs.II-2-5 and II-2-6, a magnetic anomaly map is shown in Fig.II-2-7.

In this area, magnetic anomaly distribution shows a remarkable difference between the Southern Kinabalu and Labuk areas. That is, large-scale high magnetic anomalies of long wave-length are distributed bloadly in the Southern Kinabalu area, and on the other hand, smale-scale low magnetic anomalies of short wave- length are dominated in the Labuk area. This seems to reflect the differences of geology and/or geological structures between the both areas.

1) Southern Kinabalu area

In the high magnetic anomalous zone in the Southern Kinabalu area, the values of total field magnetics increase towards the southeast.

Contour lines trending in an NE-SW direction are distributed predominantly, and those of NW-SE, NS to NNW-SSE, and EW directions are dominated in the

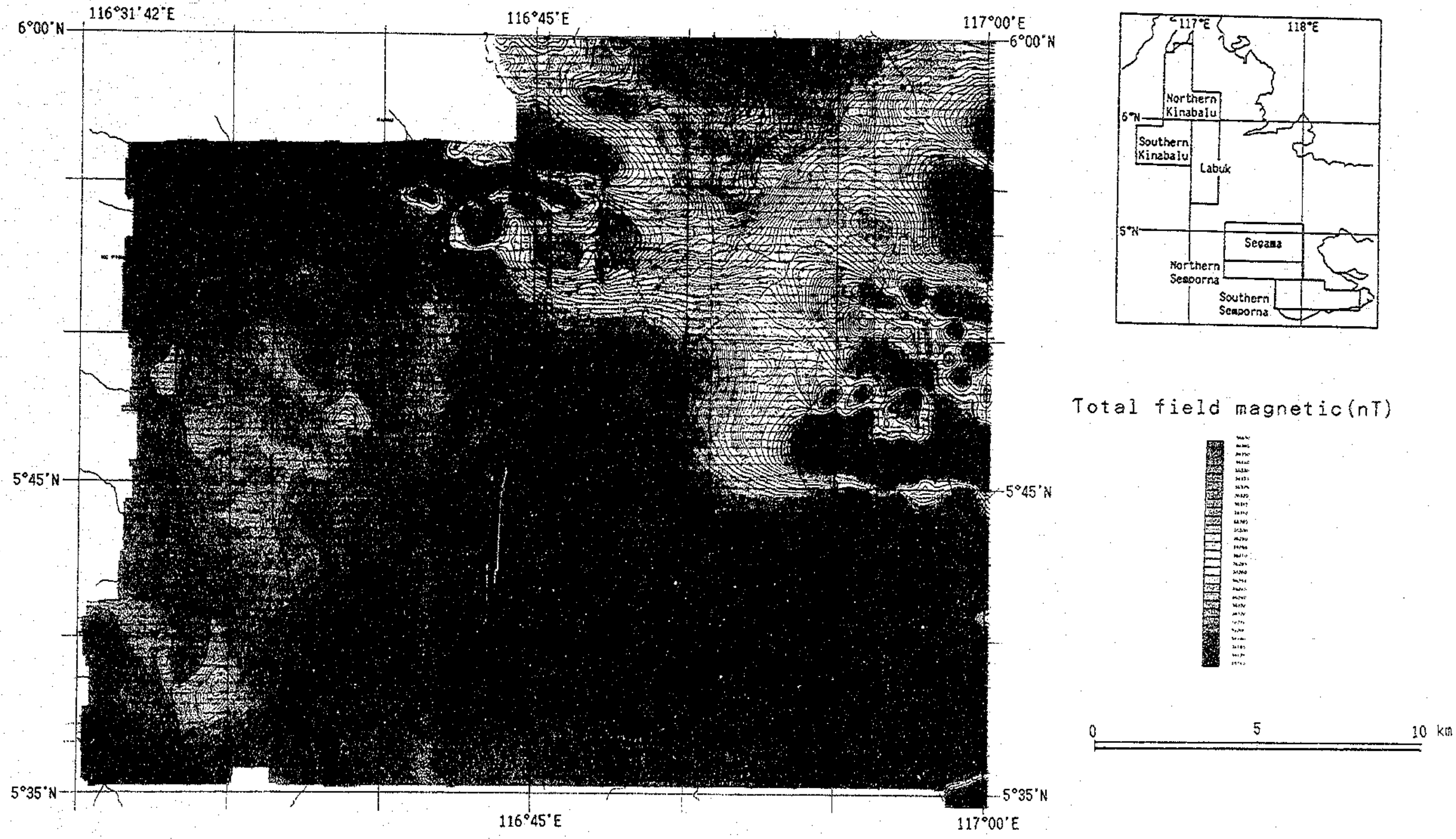

Fig. II-2-5 Total field magnetics the Southern Kinabalu area

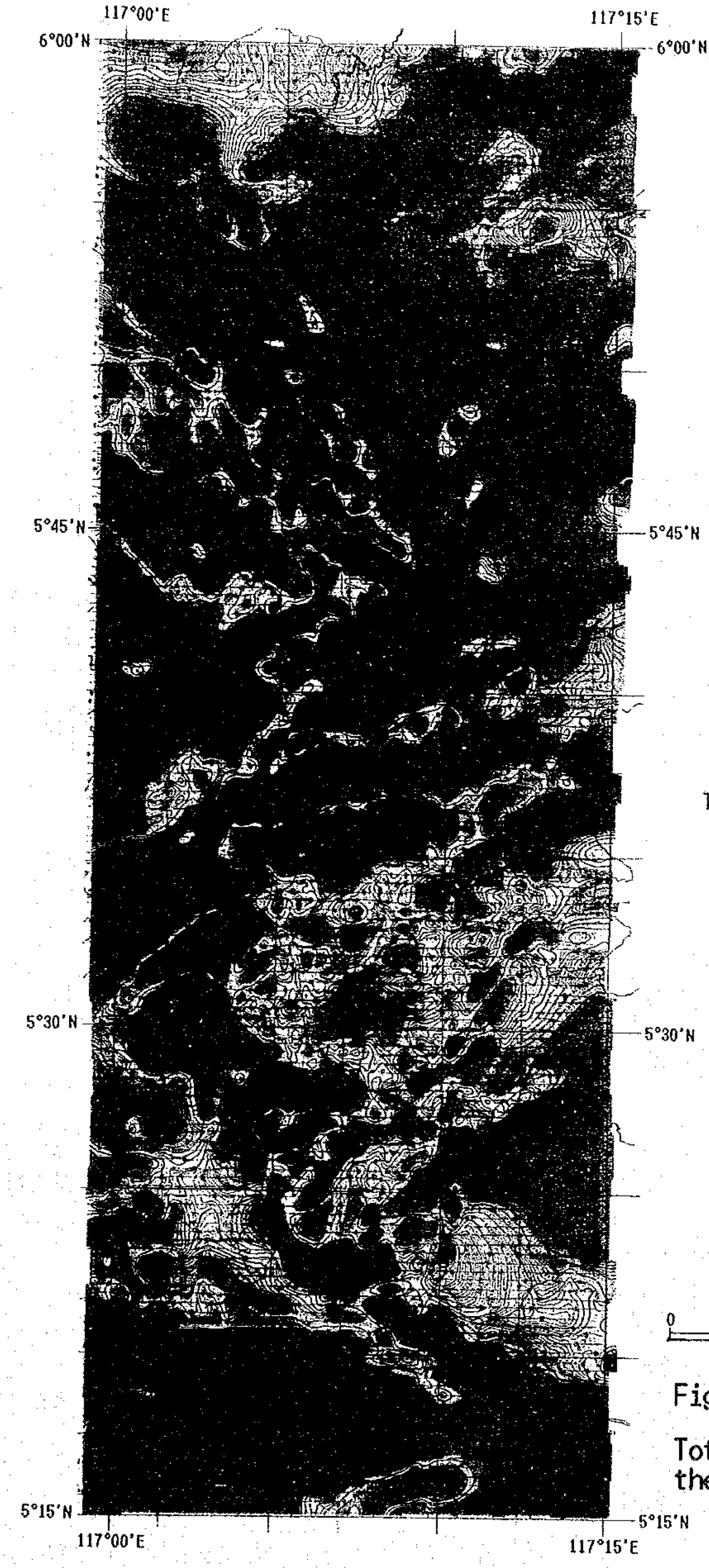

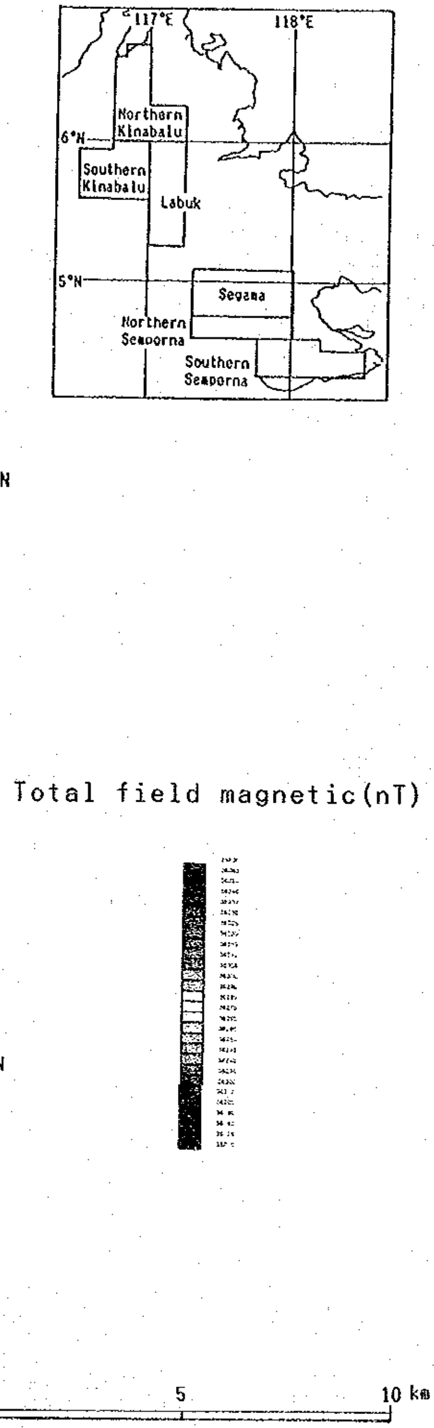

Fig. II-2-6

Total field magnetics of the Labuk area

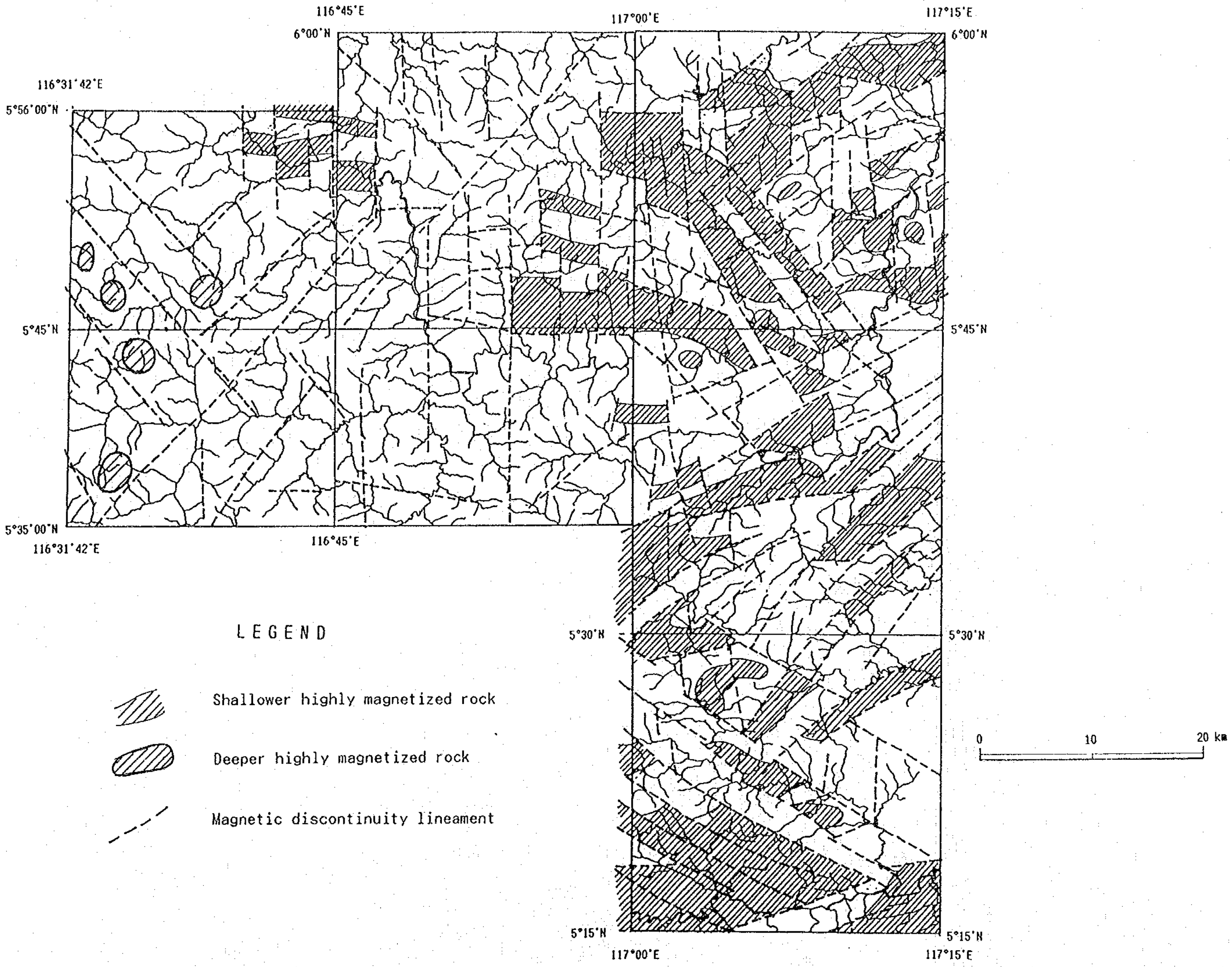

Fig. II-2-7 Magnetic anomaly map of the Southern Kinabalu and Labuk area

western, central-to-northern and central-to-southern parts, respectively.

And magnetic anomalies of relatively long wave-length and small amplitude show alignments in NW-SE, N-S and E-W directions at the western, central-to-southeatern and southern parts. These magnetic anomalies seem to be caused by highly magnetized rocks(intrusive rocks) at the deep. According to the results of curve matching method, these magnetic anomalies are caused by highly magnetised bodies of the depths of 1 - 2 km below ground level and the susceptibilities of 0.2 - $0.7x10^{-3}$CGSemu, corresponding to dacite and/or gabbro.

At the north of this high anomalous zone, there is found a part of a long wave-length and large-scale low magnetic anomaly. While at the northwest end short wave-length magnetic anomalies of large amplitude are distributed, which are thought to be induced by magnetized rocks at and near the ground surface.

2) Labuk area

Short wave-length magnetic anomalies are dominated in the Labuk area, which show characteristic alignments of NNW-SSE to NW-SE, NE-SW, NE-SW to ENE-WSW, and NW-SE to WNW-ESE directions in the northern, northeastern, central, and southern parts, respectively. These alignments reflect the geology and geologic structure.

At the northwestern part, short wave-length anomalies of relatively large amplitude align in a direction of NNW-SSE to NW-SE, which suggest the existence of highly magnetized rocks near ground surface and magnetic discontinuity lineaments with the same direction. And these highly magnetized rocks are divided into small blocks by N-S trending magnetic discontinuity lineaments.

At the northeastern part, magnetic anomalies of small amplitude align in the NE-SW direction, and the causative bodies seem to show weaker magnetization than those at the northwestern part. The magnetized bodies are also divided into small blocks by N-S trending magnetic discontinuity lineaments similarly as at the northwestern part.

At the western side of the central part, low magnetic anomalies of relatively large amplitude surround the large high magnetic anomalous zone and align in NW-SE and NE-SW to ENE-WSW directions at the north and south of the zone, respectively, which suggest the existence of highly magnetic bodies of relatively large scale. On the other hand, at the eastern side, high magnetic anomalies of small amplitude dominated, and small-amplitude magnetic anomalies of short wave length align in ENE-WSW direction, which are caused by relatively low magnetized bodies trending in the same direction.

At the southern part, short wave-length magnetic anomalies align in NW-SE to WNW-ESE directions, caused by highly magnetised rocks near ground surface. And there are found many magnetic discontinuity lineaments trending in NW-SE to WNW-ESE and N-S to NE-SW directions.

And relatively large-scale low magnetic anomalies are found at the south end, caused by highly magnetized bodies of large scale near ground surface and at the shallower part.

② Radiometric anomaly map

Radiometrics total count contour maps and ternery maps of the Southern Kinabalu area and the Labuk area are shown in Figs.II-2-8 and II-2-9, and Figs.II-2-10 and II-2-11, respectively. And a radiometric anomaly map of the Southern Kianbalu and Labuk area is shown in Fig.II-2-12.

Radiometric anomaly distribution shows a similar characteristic pattern as magnetic anomaly distribution. That is, high total count radiometric anomalous zone occupies the Southern Kinabalu area. On the other hand, in the Labuk area, low total count radiometrics are dominated and high total count anomalies are isolated.

1) Southern Kinabalu area

Very high total count zones are found at the central to southwestern part in a high total count zone.

As a potassium(K) high count zone coincide almost with a high total count zone, the total count radiometrics in this zone are contributed by pottasium mainly. While, there are small-scale uranium(U) high count anomalies in the central to southwestern part, where uranium radiometrics also contribute to total count radiometrics.

2) Labuk area

The Labuk area is occupied by low total count radiometrics, and high total count radiometrics are found bloadly at the northeastern, southeastern, southwestern and southern parts, and scarcely at the central part. Those, except for that at the southern part, align in NNW-SSE, N-S and NNE-SSW directions.

Potassium(K) high count radiometrics are distributed bloadly at the northeastern and southern parts, where total count radiometrics are contributed by

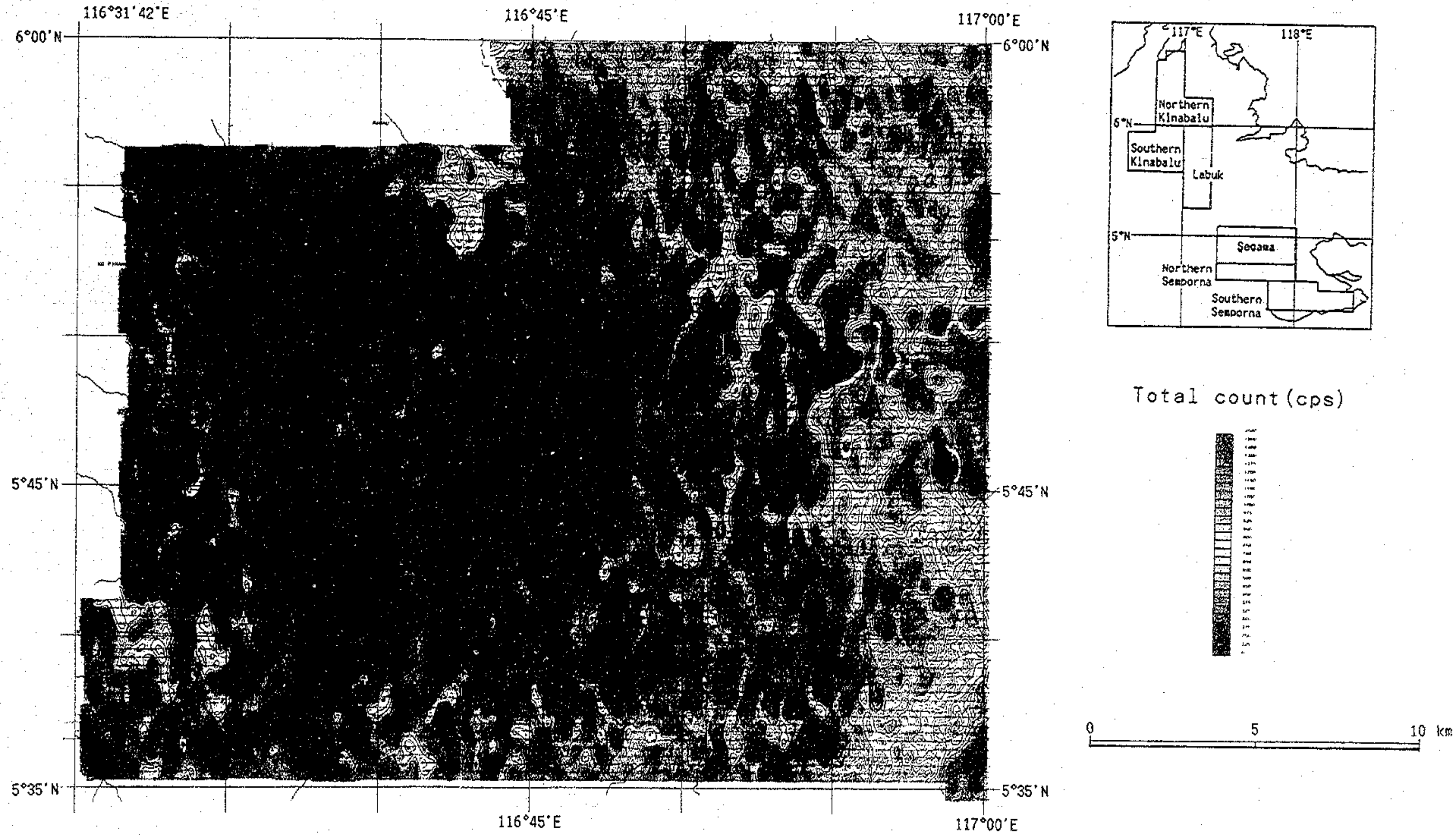

Fig. II-2-8 Radiomeric total count of the Southern Kinabalu area

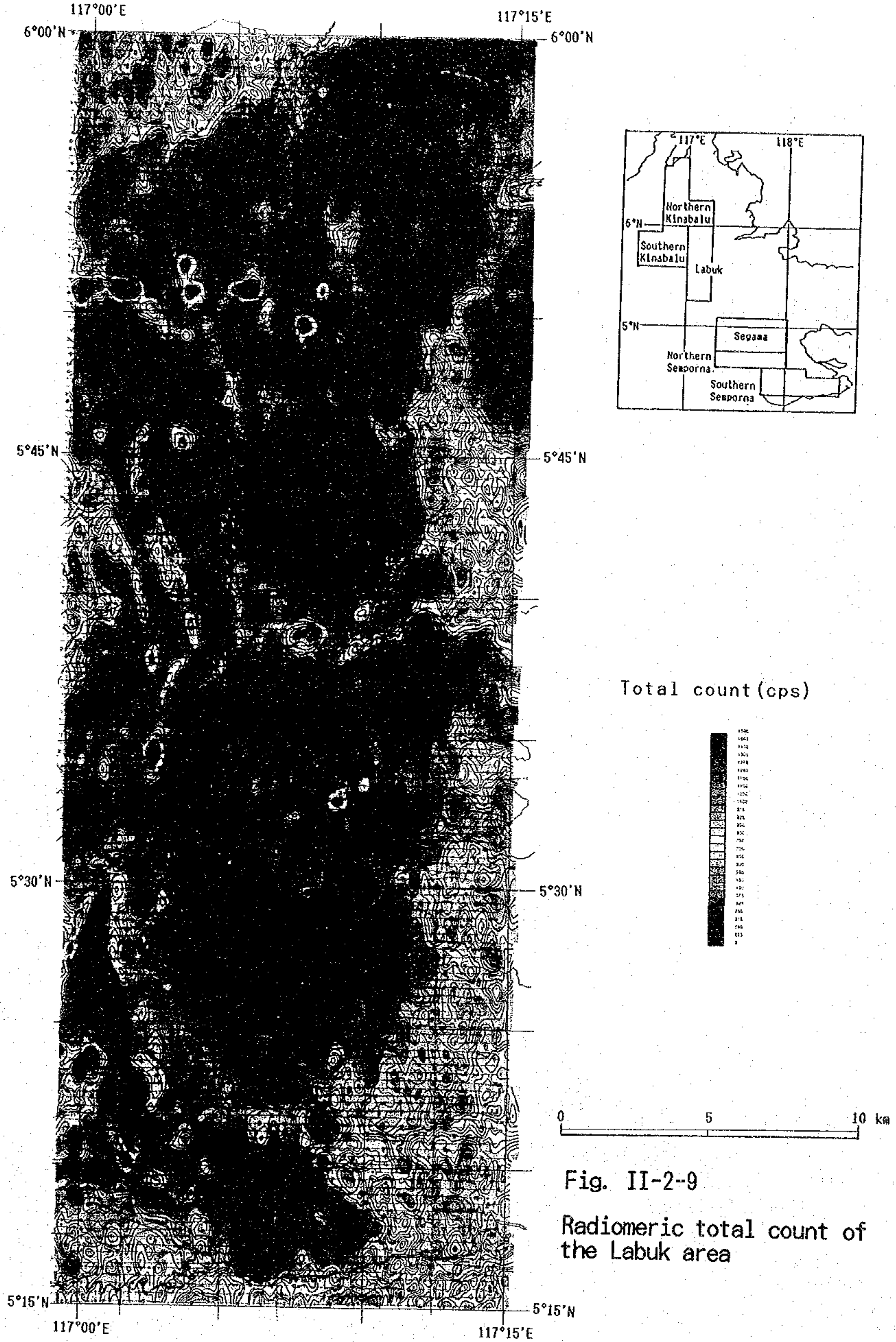

Fig. II-2-9

Radiomeric total count of the Labuk area

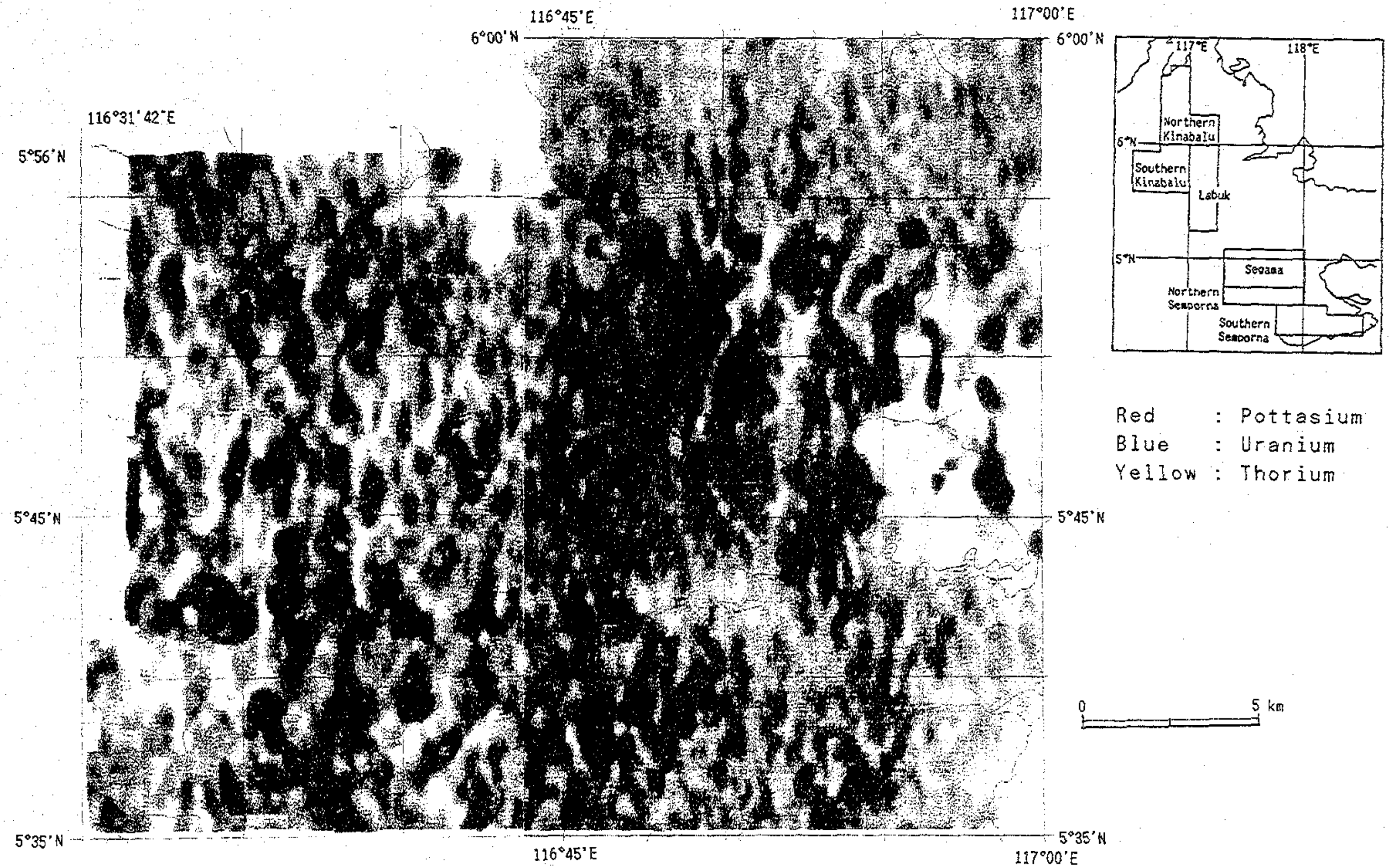

Fig. II-2-10 Radiomeric ternery map of the Southern Kinabalu area

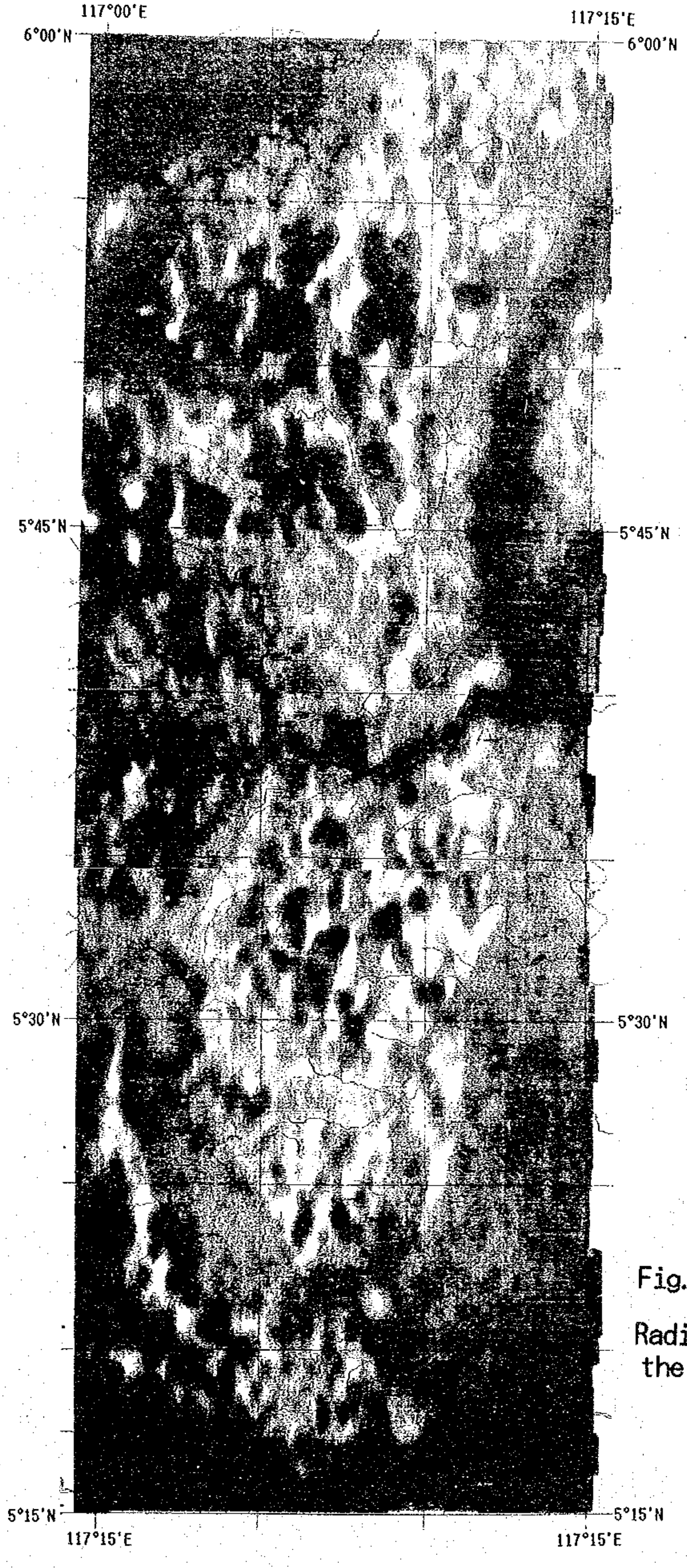

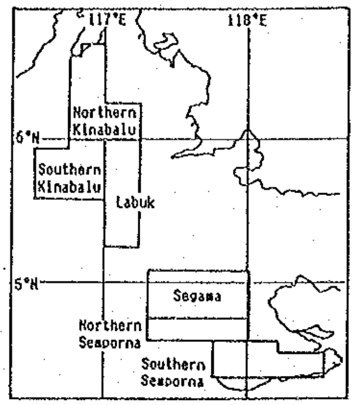

Red : Pottasium
Blue : Uranium
Yellow : Thorium

0 5 km

Fig. II-2-11

Radiomeric ternery map of the Labuk area

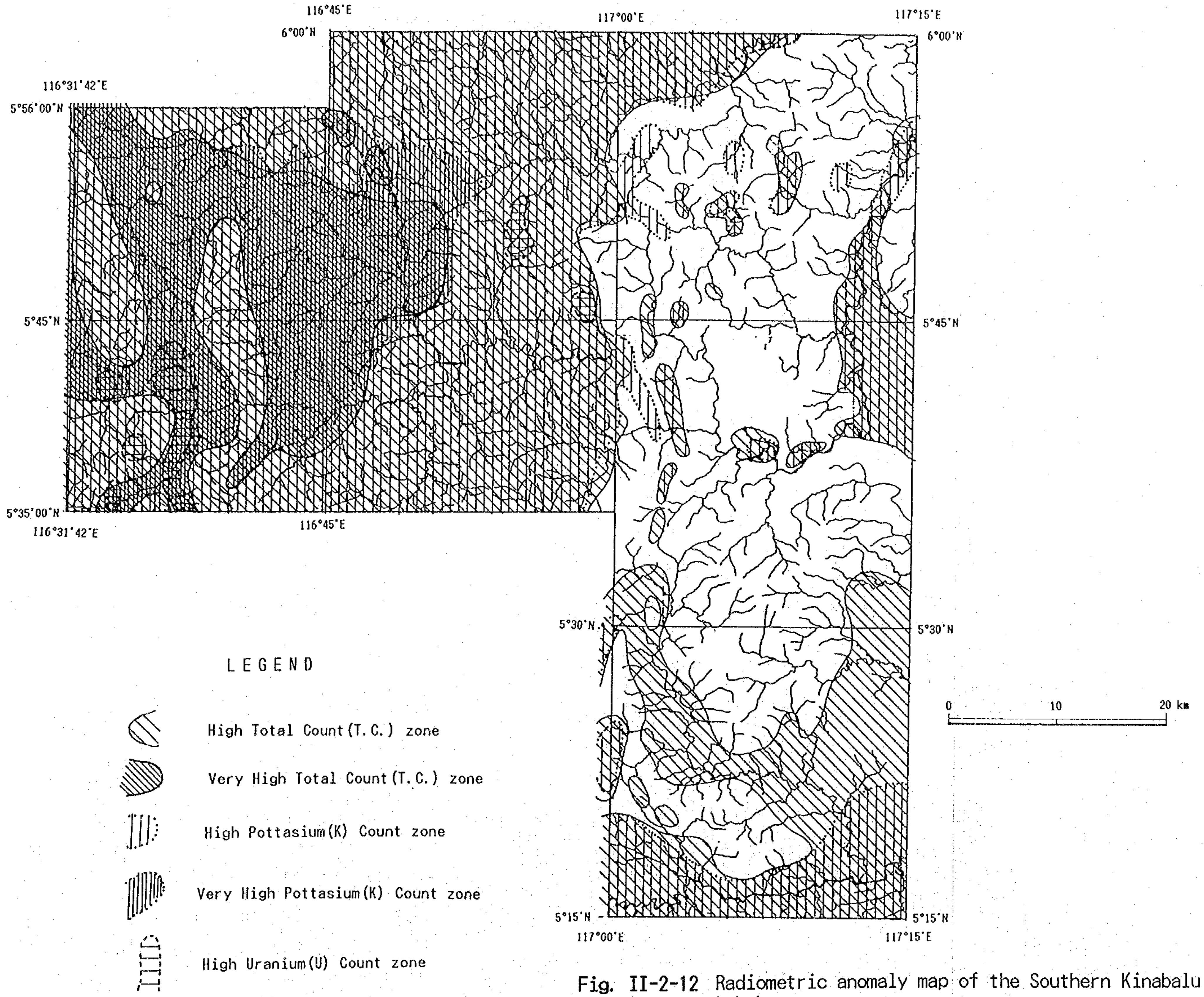

Fig. II-2-12 Radiometric anomaly map of the Southern Kinabalu and Labuk area

potassium mainly. Uranium(U) shows low count wholly in the this area, but there are small-scale uranium high count anomalies in the central part. And thorium (Th) high count zones are concentrated at the southeastern and southwestern parts, where thorium contributes to total count radiometrics mainly.

(2) Segama and Semporna area

① Magnetic anomaly map

Total field magnetic maps of the Segama, Northern Semporna and Southern Semporna areas are shown in Figs.II-2-13, II-2-14 and II-2-15, a magnetic anomaly map of the Segama and Semporna area is shown in Fig.II-2-16.

Total field magnetic maps show the following characteristic distribution pattern:

i) Northern part(Segama area);

E-W trending low magnetic anomalies of long wave length and large amplitude are distributed predominantly.

ii) Central part(Northern Semporna area);

High magnetic anomalies of long wave length are dominated.

iii) Southwestern part(Southern Semporna area);

Low magnetic anomalies of short wave length are distributed bloadly at the south of circular pattern.

iv) Southeastern part(Southern Semporna area);

E-W trending low magnetic anomalies are found.

1) Northern part(Segama area)

E-W trending magnetic anomalies of large amplitudes and a lot of small-scale magnetic anomalies are distributed at the northern part, and the western and eastern parts, respectively, which are caused by ultra-basic rocks at the ground surface. Magnetic discontinuity lineaments trending in E-W and NE-SW are found predominantly, by which highly magnetized bodies are divided into a lot of small blocks.

There are high magnetic anomalies of long wave length at the western-to-southwestern part, reflecting the distribution of non-magnetic sedimentary rocks. And in the southwestern part, magnetic anomalies of small amplitude and relatively short wave length are found in the southwestern high-magnetic anomalies.

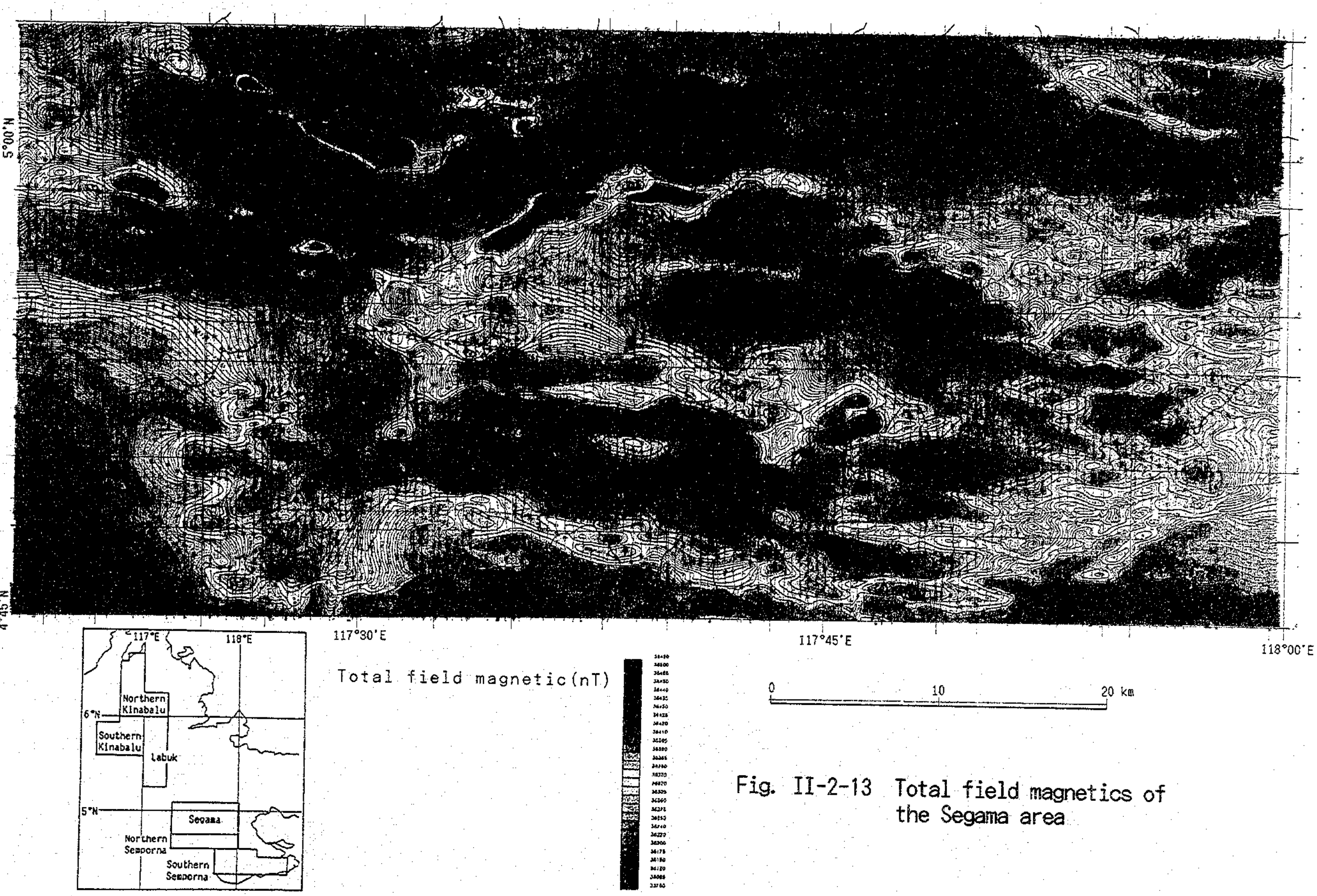

Fig. II-2-13 Total field magnetics of the Segama area

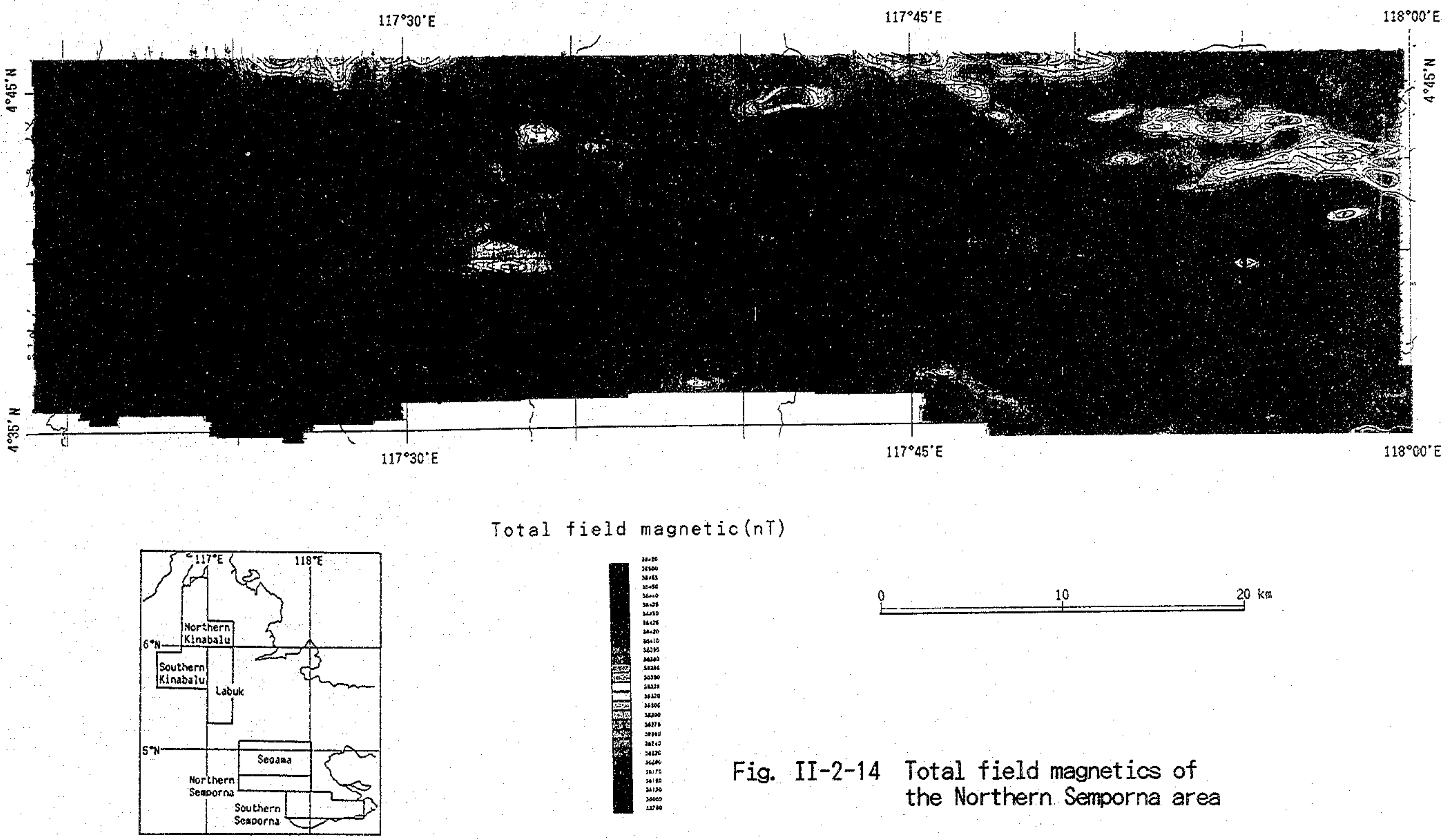

Fig. II-2-14 Total field magnetics of the Northern Semporna area

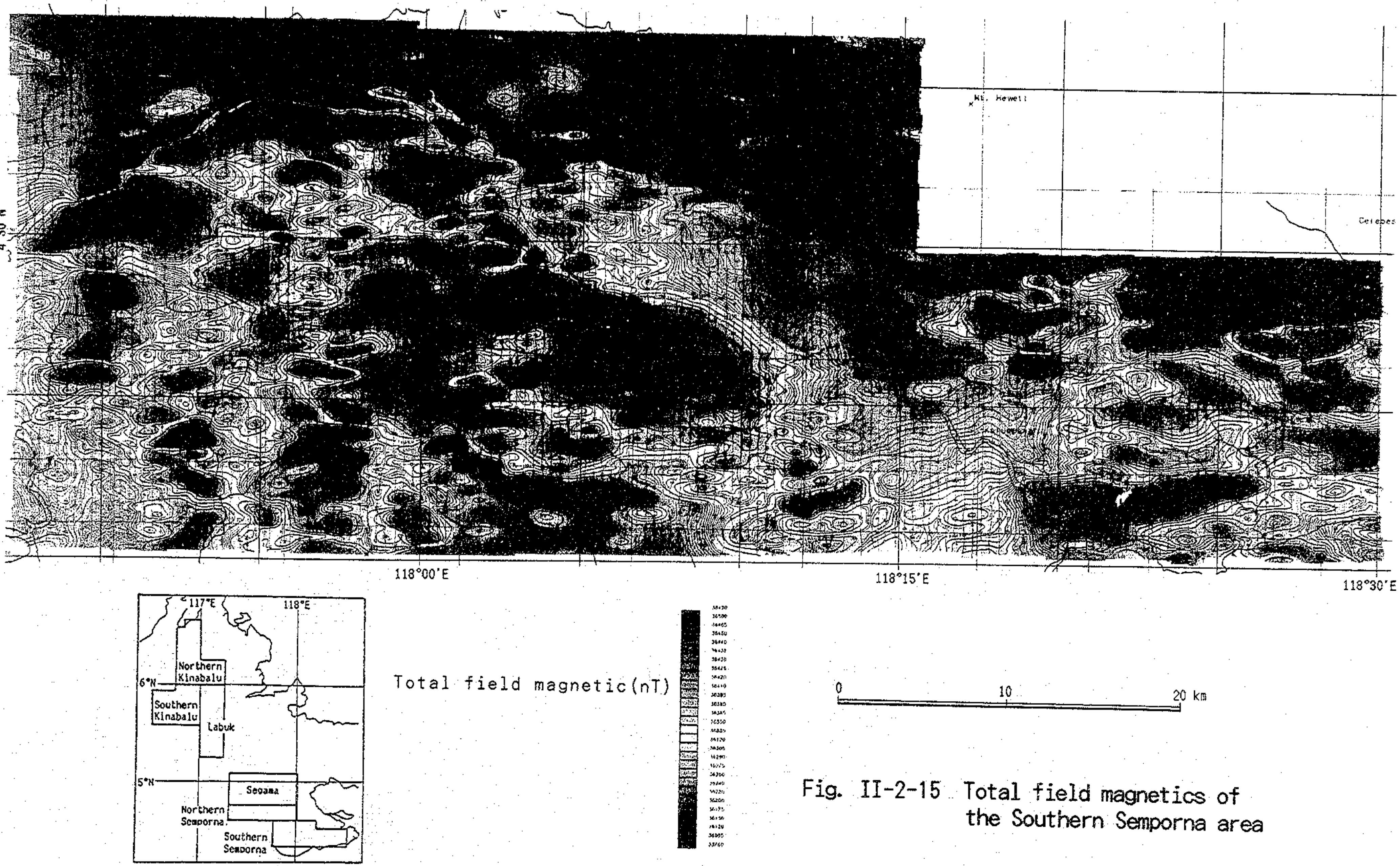

Fig. II-2-15 Total field magnetics of the Southern Semporna area

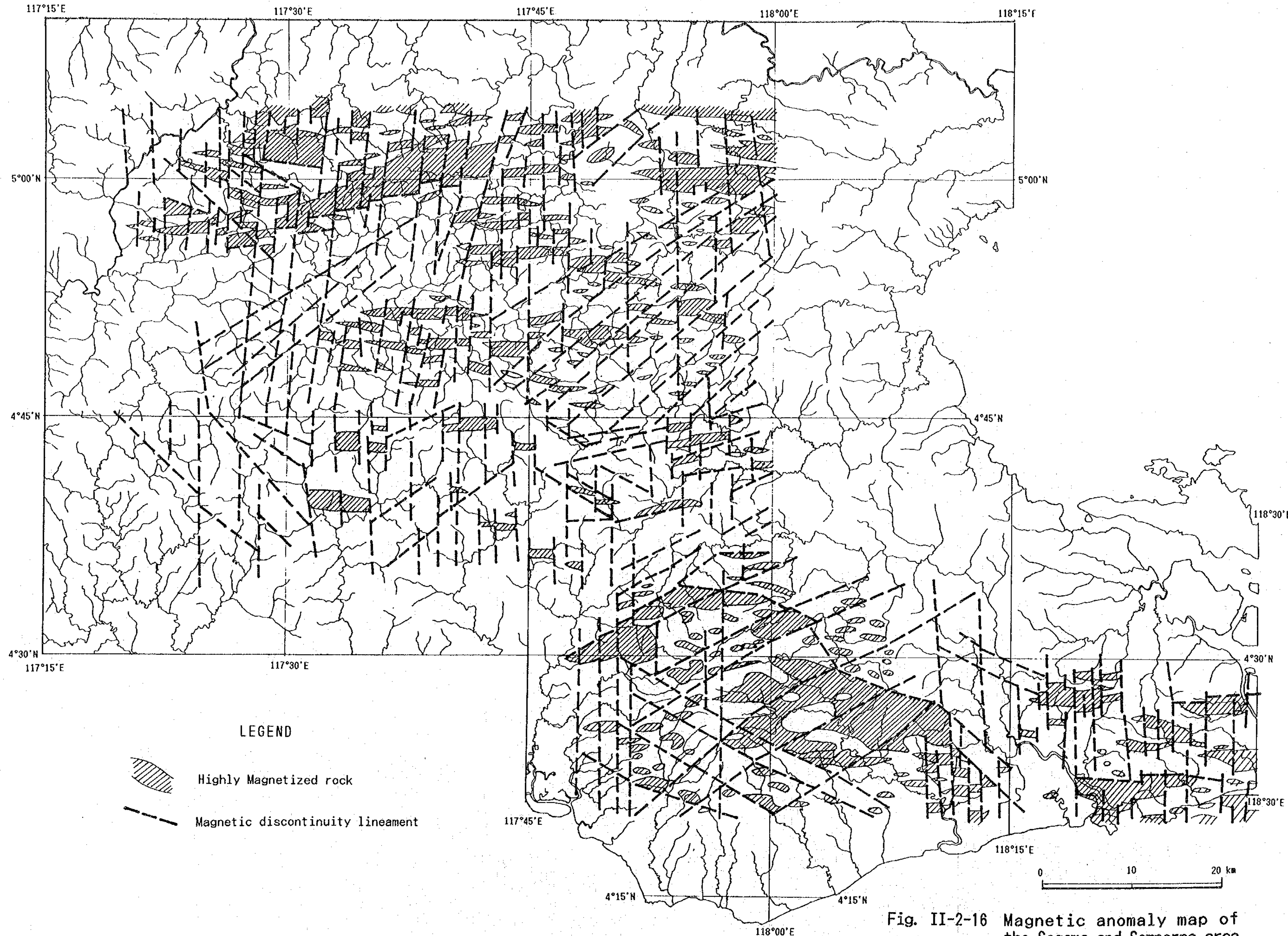

Fig. II-2-16 Magnetic anomaly map of the Segama and Semporna area

Those small anomalies suggests the existence of highly magnetized bodies at the shallower part, corresponding to intrusive rocks of ultra-basic rocks. Moreover, these highly magnetized bodies are divided into small blocks by magnetic discontinuity lineaments trending in the NE-SW to ENE-WSW directions.

2) Central part (Northern Semporna area)

This part is occupied by high magnetic zone wholly, and this suggests non-magnetic sedimentary rocks are dominated. Magnetic discontinuity lineaments reflecting the geologic structure are found as follows; N-S trending lineaments in the whole part, NW-SE trending ones at the western part and NE-SW to ENE-WSW trending ones at the central-to-eastern part.

At the central-to-eastern part, there are found a lot of magnetic anomalies of small amplitude and relatively long wave length suggesting the existence of highly magnetized bodies at the shallower part. These highly magnetized bodies seem to correspond to ultra-basic rocks which intruded into the sedimentary rocks

3) Southwestern part (Southern Semporna)

This area is located at the south of high magnetic anomalous zone of the Northern Semporna area, and magnetic anomalies of large amplitude are distributed showing circular pattern opened southward. At the south of circular pattern, there are found a lot of low magnetic anomalies of short-to-long wave length. At the western side of the area, magnetic changes are very small so that it suggests non-magnetic rocks such as sedimentary rocks are dominated.

Magnetic discontinuity lineaments trending in N-S, NW-SE and NE-SW directions are distributed in this area.

The north end of the circular pattern is limitted by NW-SE and NE-SW trending magnetic discontinuity lineaments. And a lot of low magnetic anomalies of long-to-short wave length are distributed at the south of the circular pattern, which are due to highly magnetized bodies such as andesite at the ground surface. And these bodies extend toward the southeast, but decrease those sizes.

4) Southeastern part (Southern Semporna)

There are found low magnetic anomalies of large amplitude extending in E-W directions, reflecting the existence of highly magnetized bodies such as andesite at the ground surface. These highly magnetized bodies are divided into small blocks by N-S trending magnetic discontinuity lineaments.

② Radiometric anomaly map

Radiometrics total count contour maps and ternery maps of the Segama, Northern Semporna and Southern Semporna areas are shown in Figs.II-2-17, II-2-18 and II-2-19, and Figs.II-2-20, II-2-21 and II-2-22, respectively. And a radiometric anomaly map of the Segama and Semporna area is shown in Fig.II-2-23.

Radiometric total count distribution shows the following characteristic pattern:

i) Northern part(Segama area);

Low total count zones are dominated and high count zones are found at the western side.

ii) Central part(Northern Semporna area);

This part is occupied by high total count anomalous zone.

iii) Southwestern and southeastern part(Southern Semporna area);

Many high count anomalies are distributed.

These features seem to reflect surface geology of each part.

1) Northern part(Segama area)

This part is occupied by low total counts except the western side, and small-scale high count anomalies are isolated, which are contributed by pottaium only. There are found many radiometric discontinuity lineaments trending in NW-SE to WNW-ESE and NE-SW to ENE-WSW directions.

On the other hand, at the western side, there are distributed high total count anomalies controlled by NW-SE to WNW-ESE trending radiometric discontinuity lineaments. Uranium high count anomalies are found at the same locations of high total count anomalies, where contribution of uranium to total count occupy very large portion. These high uranium count anomalies extend to the western side of the central part(Northern Semporna area).

2) Central part(Northern Semporna area)

This part is occupied by high total count zone, corresponding to the sedimentary rocks. Radiometric discontinuity lineaments are distributed in the direction of NW-SE at the central, and E-W, NW-SE and NE-SW. And spotted low-count zones are found where highly magnetized bodies such as ultra-basic rocks are existed at the ground surface and/or at the shallower part. Except for the western side, uranium high count anomalies of small scale are spotted and total

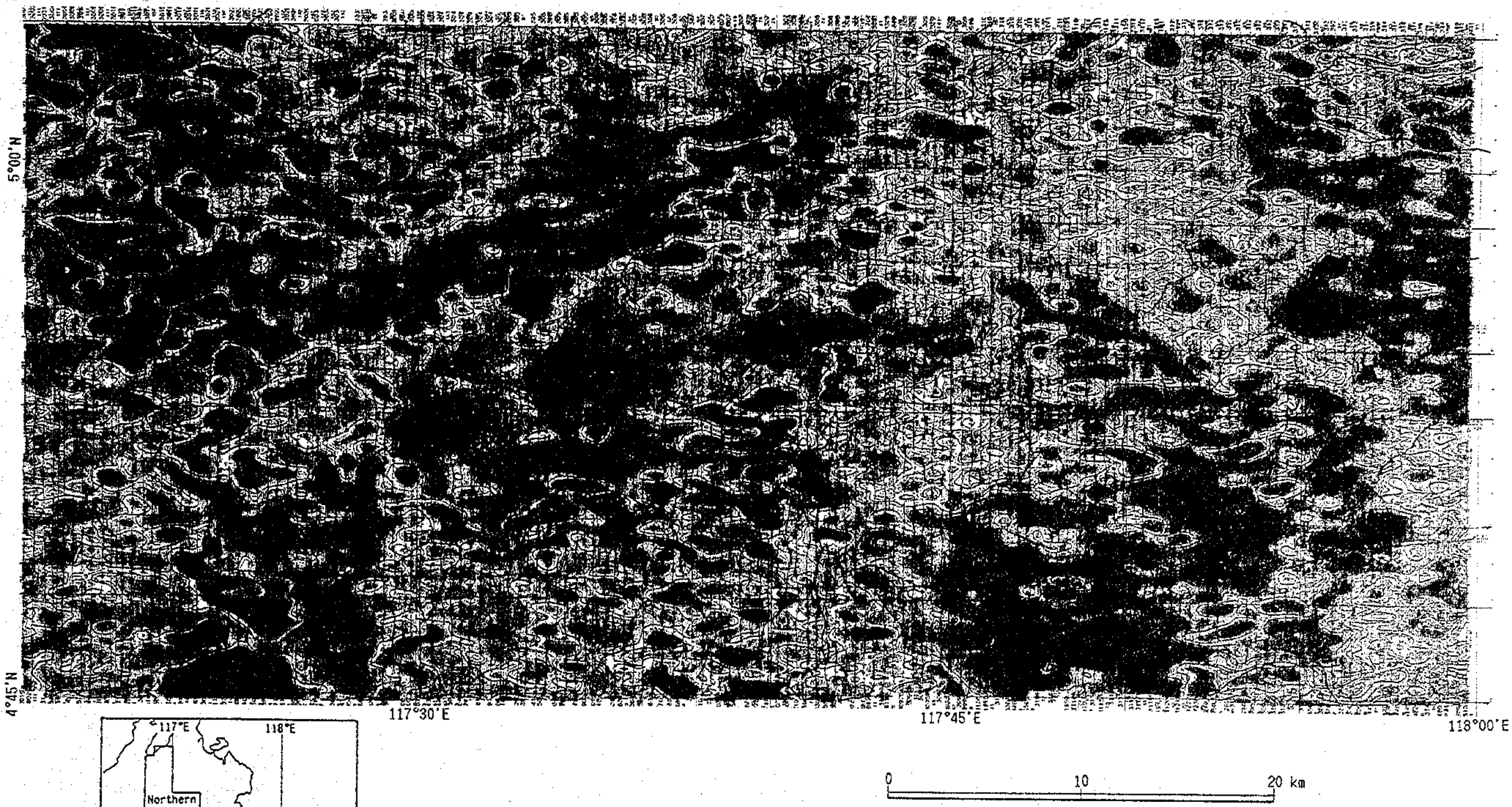

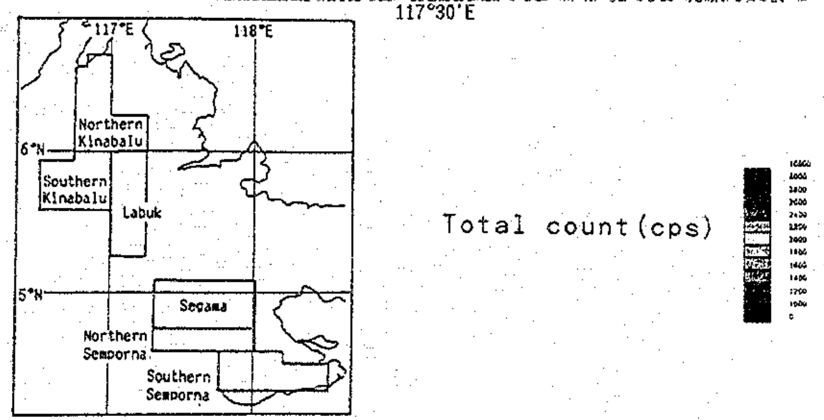

Fig. II-2-17 Radiomeric total count of the Segama area

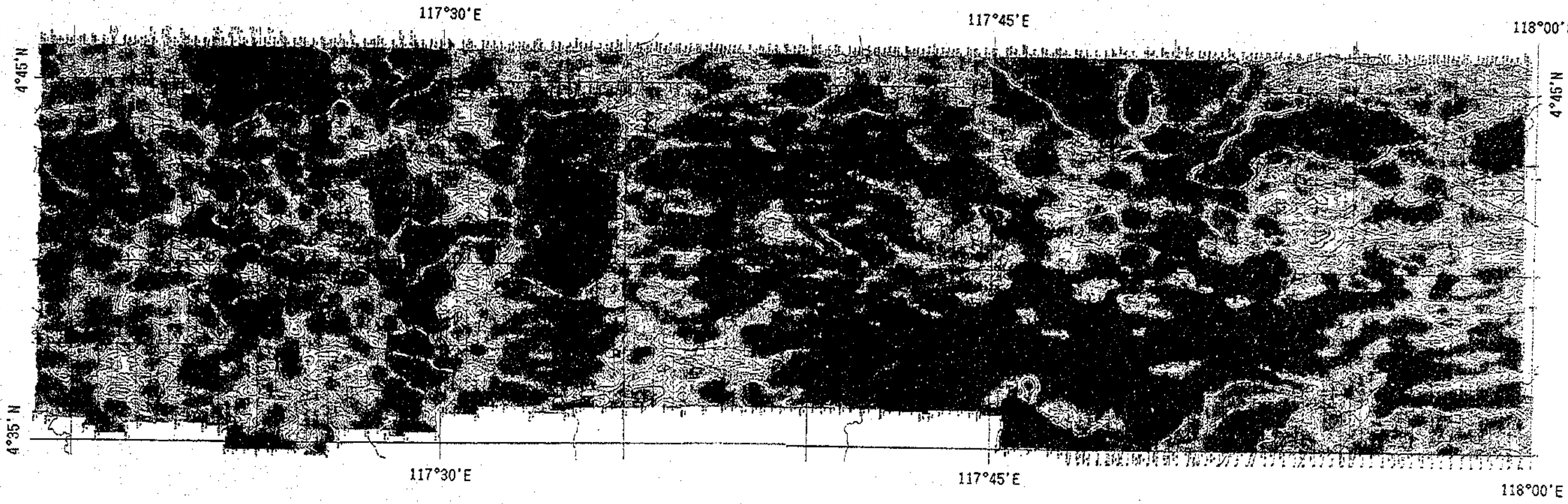

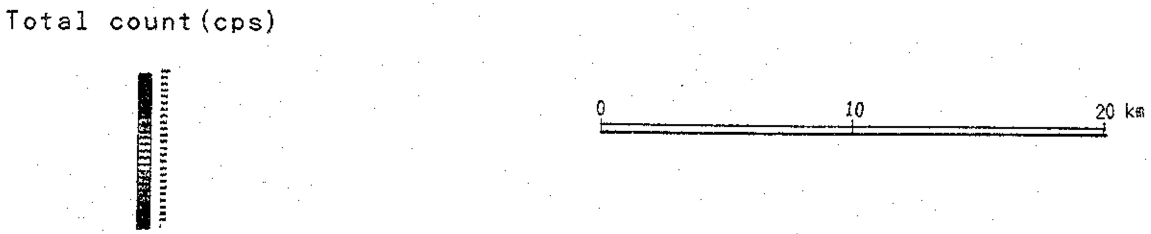

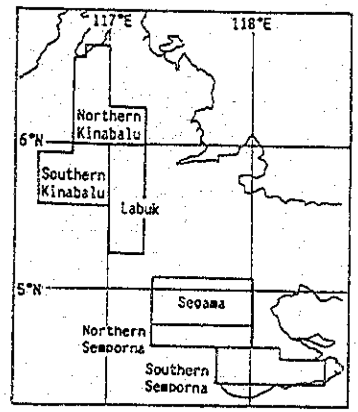

Fig. II-2-18 Radiomeric total count of the Northern Semporna area

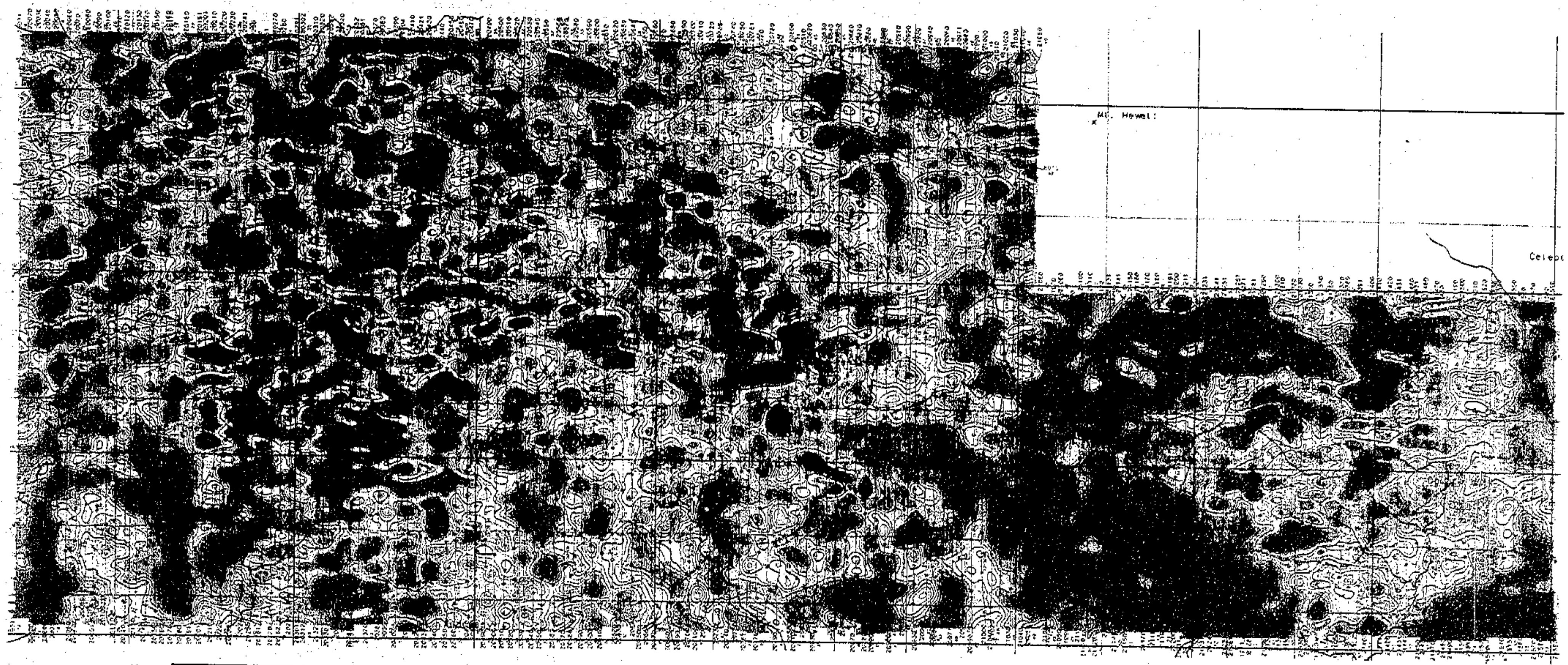

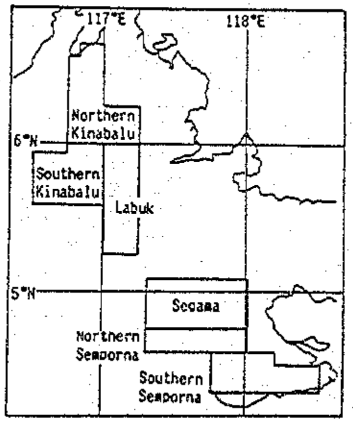

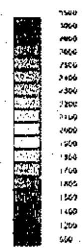

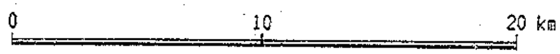

Fig. II-2-19 Radiomeric total count of the Southern Semporna area

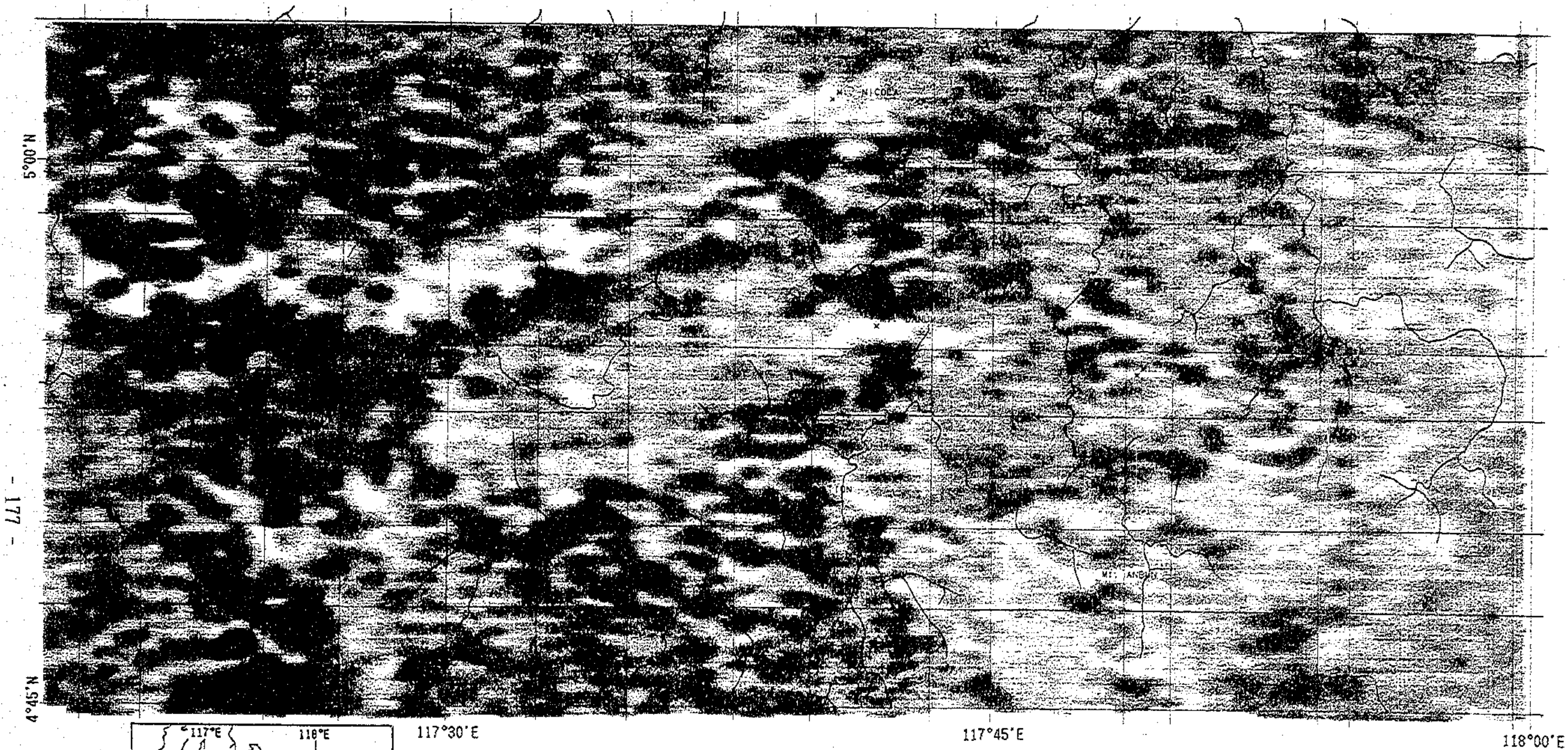

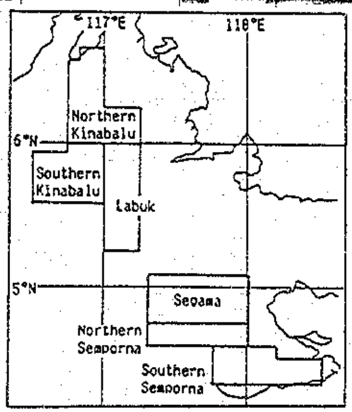

0 10 20 km

Red : Pottasium
Blue : Uranium
Yellow : Thorium

Fig. II-2-20 Radiomeric ternery map of the Segama area

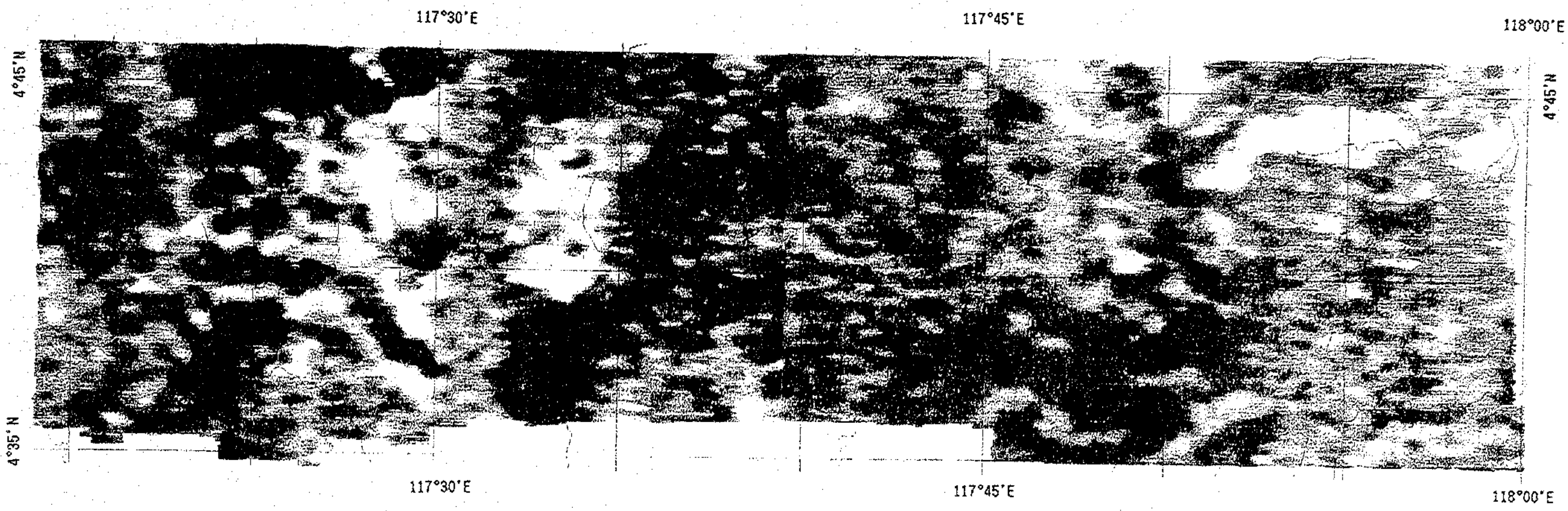

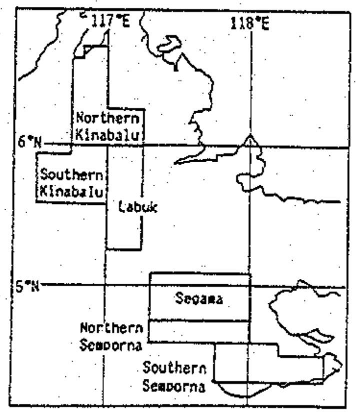

Red : Pottasium
Blue : Uranium
Yellow : Thorium

0 10 20 km

Fig. II-2-21 Radiomeric ternery map of the Northern Semporna area

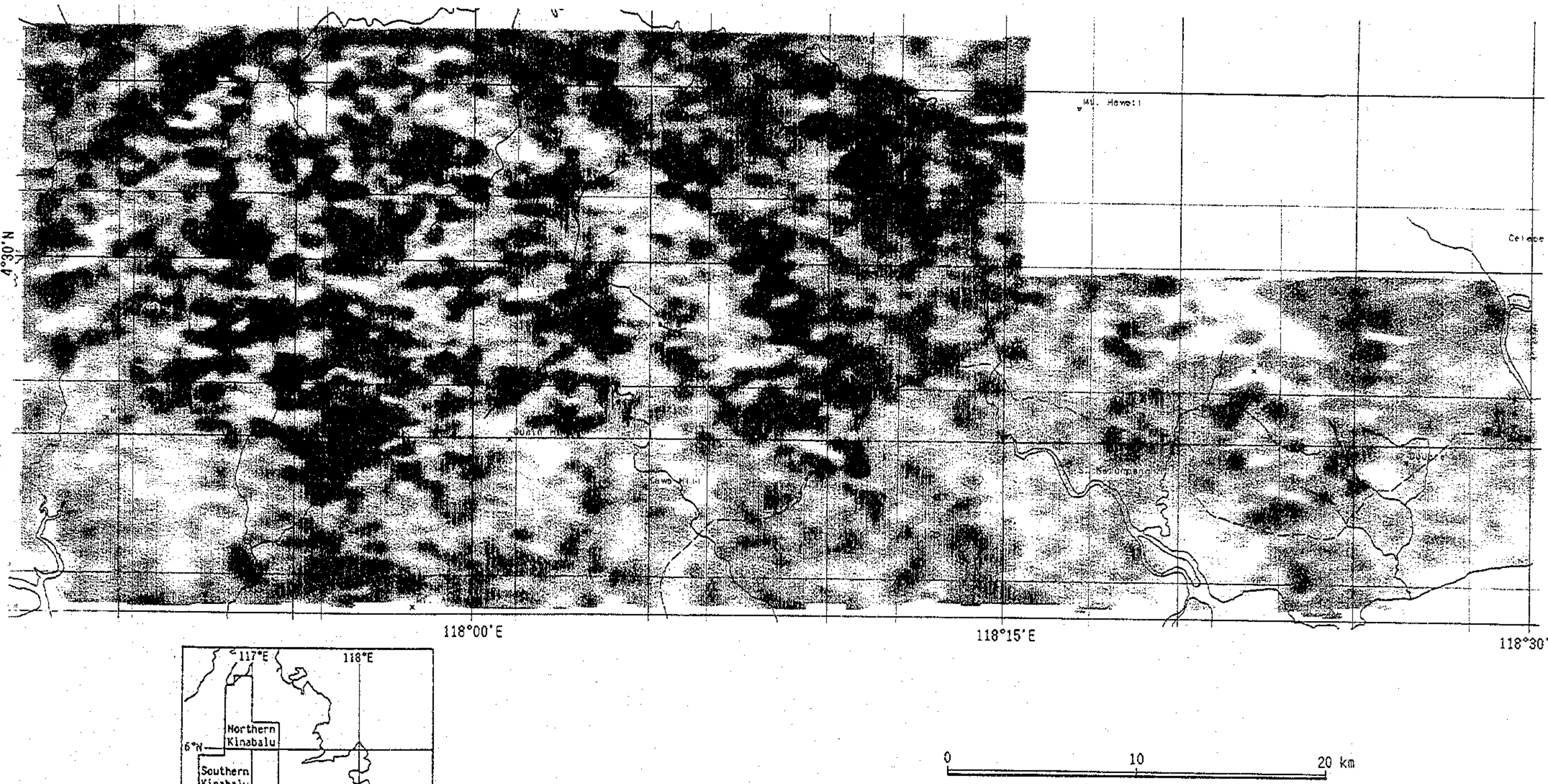

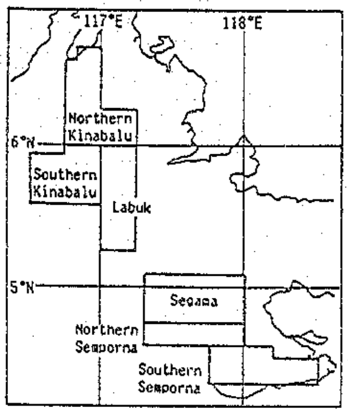

Red : Pottasium
Blue : Uranium
Yellow : Thorium

Fig. II-2-22 Radiomeric ternery map of the Southern Semporna area

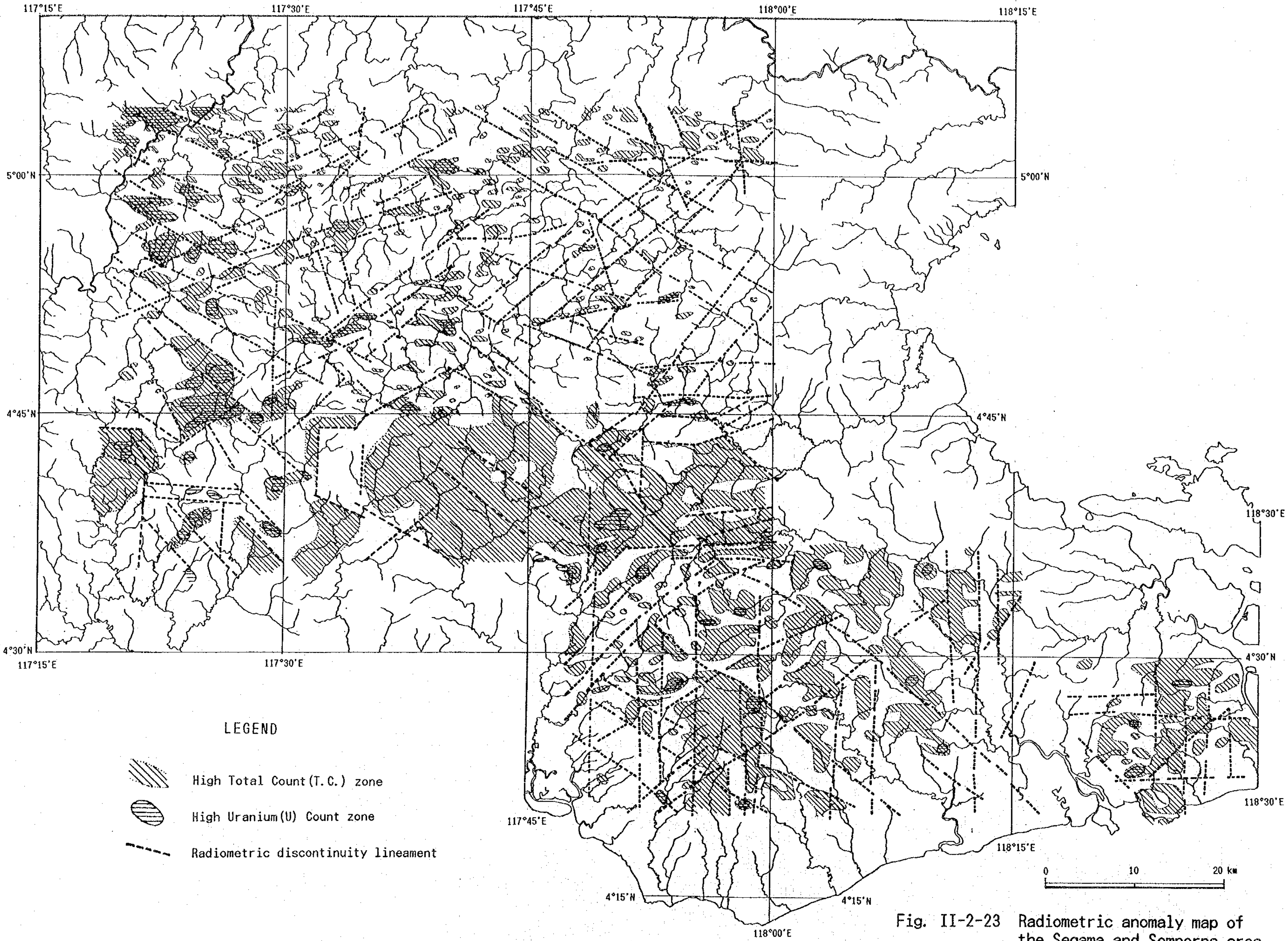

Fig. II-2-23 Radiometric anomaly map of the Segama and Semporna area